Hyperglycemia-induced alteration of ER redox homeostasis delays ER export of proinsulin

Kristen E. Rohli[1,2,3], Cierra K. Boyer[1,3,4], Shelby C. Bearrows[1,3], Marshall R. Moyer[1,3], Weston S. Elison[5], Casey J. Bauchle[1,3], Sandra E. Blom[1,3], Chi-Li Yu[6], Marshall R. Pope[6], Jianchao Zhang[7], Yanzhuang Wang[7,8], and Samuel B. Stephens[1,2,3,9]

[1]Fraternal Order of Eagles Diabetes Research Center, University of Iowa, Iowa City, IA, USA
[2]Interdisciplinary Graduate Program in Genetics, University of Iowa, Iowa City, IA, USA
[3]Department of Internal Medicine, Division of Endocrinology and Metabolism, University of Iowa, Iowa City, IA, USA
[4]Department of Pharmacology, University of Iowa, Iowa City, IA, USA
[5]Department of Nutrition, Dietetics, and Food Science, Brigham Young University, Provo, Utah, USA
[6]Proteomics Facility, University of Iowa, Iowa City, IA, USA
[7]Department of Molecular, Cellular, and Developmental Biology, University of Michigan, Ann Arbor, MI, USA
[8]Department of Neurology, School of Medicine, University of Michigan, Ann Arbor, MI, USA

[9]Corresponding author:
Samuel B. Stephens, Ph.D.
Fraternal Order of Eagles Diabetes Center
Department of Internal Medicine, Division of Endocrinology and Metabolism
University of Iowa
Iowa City, IA 52246
Email: samuel-b-stephens@uiowa.edu
Tel. 319-335-4843

Running title: Hyperglycemia impairs proinsulin trafficking

Key words: ER redox, proinsulin trafficking, secretory granule formation, β-cell function

Abstract

Defects in the β-cell's secretion system are well-described in Type 2 diabetes (T2D), including reduced insulin storage and impaired proinsulin processing; however, the cellular mechanisms underlying these secretory defects and the contribution of chronic hyperglycemia to this process remain poorly understood. In this study, we provide evidence that oxidative protein folding in the endoplasmic reticulum (ER) is perturbed in models of β-cell dysfunction, leading to delays in proinsulin trafficking and insulin granule formation. Using an *in situ* fluorescent pulse-chase labeling strategy and APEX2-based proximity labeling, we demonstrate that enriched interactions of proinsulin with ER oxidoreductases coincides with a delay in proinsulin ER export. Furthermore, our data show that proinsulin ER export can be regulated by metabolically derived NADPH and reducing equivalent (glutathione) availability. Together, these data highlight an emerging role for nutrient metabolism and mitochondrial dysfunction in the maladaptive remodeling of the β-cell's secretory pathway during the decline of β-cell function in T2D.

Introduction

In the pancreatic islet β-cell, metabolic fuel sensing functions at multiple levels to coordinate insulin secretory capacity with physiological demands of nutrient status[1]. For example, ATP and other metabolic signals generated by glucose oxidation directly trigger and amplify insulin granule exocytosis through membrane depolarization and insulin granule recruitment [2–4]. In addition, mitochondrial metabolism of glucose and other fuels stimulates the translation of preproinsulin mRNA through a stem-loop structure in the 5'UTR, as well as ~50 other mRNAs associated with insulin granules[5–7], to ensure that β-cells meet or exceed the physiological demands of insulin release with insulin granule biosynthesis. More global changes in β-cell secretory function can also occur, such as in response to prolonged fasting, which results in a pronounced impairment in the β-cell's insulin secretory capacity, including insulin degranulation and increased autophagosomes and lysosomes, as part of a physiological mechanism to ward off hypoglycemia[8]. Taken together, these observations illustrate the β-cell's ability to use metabolic fuels as hierarchal signals to modulate secretory functions.

Loss of β-cell secretory function and insulin insufficiency have been identified as critical events in the progression of insulin resistance to Type 2 diabetes (T2D), yet the underlying cellular mechanisms are not well understood[9,10]. Overt changes in the β-cell's secretory pathway accompany the onset of T2D and include reduced numbers of insulin-containing secretory granules, proinsulin processing deficiencies, and hyperproinsulinemia[11–15]. While increased insulin exocytosis and proinsulin/insulin degradation likely contribute to the overall deficit in available insulin supply in T2D[16–18], perturbations in the ultrastructure of the β-cell secretory

organelles (ER, Golgi, autophagosomes) suggest that alterations in early stages of proinsulin sorting and trafficking also contribute to the insulin insufficiency in T2D[11,12,15]. Studies on early stages of proinsulin trafficking and insulin granule formation have been challenging, in part, due to the prolonged half-life of proteins within the mature secretory granule, such as insulin (t ½ ~ 2.7 days)[19], which are also highly abundant. Nevertheless, defects in proinsulin trafficking and insulin granule formation can directly decrease insulin secretory capacity[20–22] and may occur in T2D[23].

Insulin is initially synthesized as the prohormone precursor, proinsulin, which is folded via the assistance of ER resident chaperones, such as BiP[24] and GRP94[25,26], while protein disulfide isomerases (PDIs), including Pdia1 and Prdx4, facilitate formation of the three critical disulfide bonds necessary for mature insulin structure[27–29]. To maintain PDIs for sequential rounds of disulfide bond isomerization, reducing equivalents in the form of glutathione and/or thioredoxin act as the final electron donors[30,31], both of which are regenerated by NADPH-dependent enzymes, glutathione reductase and thioredoxin reductase, respectively. Studies in hepatocytes have identified a direct link between the generation of NADPH via TCA cycle metabolism and ER redox poise[32]. Enhanced TCA cycle flux increases NAPDH production and glutathione reduction with a corresponding increase in ER redox potential, whereas decreasing nutrient metabolism and NAPDH production leads to a more oxidizing ER lumen. Recent work in human and rodent T2D β-cells has demonstrated the formation of oligomeric aggregates of proinsulin due to mis-matched intermolecular disulfide bonds[29,33], highlighting that defects in ER oxidative protein folding may occur in T2D. Given the β-cell's unique metabolic fuel-sensing program, drastic alterations in ambient glucose during hyperglycemic episodes and/or defects in

mitochondrial metabolism in T2D could directly alter β-cell ER redox poise and thereby negatively impact proinsulin folding and insulin production. Indeed, impaired glucose metabolism, including diminished NADH/$FADH_2$ production, ATP synthesis, and overall oxygen consumption, have been reported in human and rodent T2D islets and coincide with reduced expression of TCA cycle enzymes and upregulation of glycolytic enzymes[34]. While previous studies have demonstrated a role for NADPH and GSH in the regulation of insulin exocytosis[35,36], the contribution of redox biology to ER function and proinsulin trafficking in the β-cell has not been investigated.

In the present study, we have evaluated proinsulin trafficking and insulin granule formation in rodent and cell culture models of hyperglycemia and T2D. Using a fluorescent pulse-chase proinsulin reporter in diabetes models, we found a significant reduction in the generation of newly synthesized insulin granules, which exhibited delayed trafficking to the plasma membrane. Using APEX2 proximity labeling to identify protein interactions with proinsulin, we found a profound increase in the enrichment of proinsulin interactions with ER oxidoreductases in β-cells cultured under hyperglycemic-like conditions, which was accompanied by diminished mitochondrial function and increased glutathione oxidation. Furthermore, we directly demonstrate a significant delay in proinsulin export from the ER in both rodent and cell culture models of T2D, which can be regulated by the availability of NADPH and reducing equivalents. Together, our data suggest that mitochondrial metabolism fails to maintain reducing equivalents necessary to support ER function in T2D β-cells, which ultimately leads to a decline in insulin granule formation.

Results

Impaired proinsulin trafficking occurs in models of β-cell dysfunction

In T2D, β-cell dysfunction is accompanied by a decline in insulin-containing secretory granules[11,12,15]. Whether alterations to insulin granule formation contribute to this deficit is not known. To address this, we evaluated proinsulin trafficking and insulin granule formation in a rodent diabetes model. For these studies, C57BL6/J mice were placed on a Western diet (WD; 40% fat/kcal, 43% carbohydrate/kcal) or standard chow (SC) for up to 8 weeks. Increased body weight (Fig. 1a) and *ad lib* fed hyperglycemia (Fig. 1b) were apparent within 4 weeks of dietary intervention and persistent for the duration of diet. Reduced glucose tolerance (Fig. 1c), fasting hyperinsulinemia, and impaired glucose-stimulated insulin release (Fig. 1d) were observed by 8 weeks of WD. Collectively, these effects are consistent with defects in β-cell function in T2D[9,10].

We previously developed an *in situ* pulse-chase fluorescent-labeling strategy to track nascent proinsulin transit through the secretory system[21] based on the modified DNA repair enzyme, SNAPtag. We inserted SNAPtag within the C-peptide region of human preproinsulin (Fig. s1a), termed proCpepSNAP, and demonstrated that the trafficking, processing, and secretion of proCpepSNAP/CpepSNAP are consistent with the regulation of endogenous proinsulin/insulin[21]. In the present study, islets were isolated from SC and WD fed mice and treated with recombinant adenovirus expressing proCpepSNAP under control of the rat insulin promoter (RIP) to ensure β-cell specific expression. Using a fluorescent pulse-chase labeling scheme to examine insulin granule formation following proinsulin exit from the Golgi[21] (Fig. s1b), we observed the

appearance of numerous nascent proinsulin (proCpepSNAP)-containing granules throughout the cell body in primary β-cells from non-diabetic, SC fed animals (Fig. 1e). In contrast, β-cells from WD fed animals displayed a substantial reduction in the total number of nascent, proCpepSNAP-labeled granules formed (Fig. 1e, f). Moreover, distance quantitation of these data revealed a significant increase in the frequency of nascent proinsulin granules within 0.5 µm of the Golgi (GM130 marker) and a decrease in granules greater than 2 µm from the Golgi in β-cells from WD compared to SC fed mice (Fig. 1e, g). Furthermore, when the diet was extended to 14 weeks, analysis by TIRF microscopy demonstrated a substantial decrease in the number of nascent (proCpepSNAP-labeled) granules trafficking to the plasma membrane in the WD model (Fig. 1h, i). Together, these data formally demonstrate an impairment in insulin granule formation and trafficking in a rodent model of diet-induced diabetes.

To further investigate alterations to insulin granule formation, we examined an insulinoma cell culture model of β-cell dysfunction. In these studies, 832/3 cells were cultured with either BSA alone or an oleate/palmitate mixture conjugated to BSA (1 mM; OP) at either normal (7.5 mM) or elevated (20 mM) glucose. Following 72 h culture, we examined insulin secretion after 1 h static incubation at basal (2.5 mM) and stimulatory (12 mM) glucose. Under these conditions, we observed no effect of fatty acid treatment alone (OP) on β-cell function, whereas elevated glucose culture alone resulted in increased basal insulin secretion. In contrast, oleate/palmitate and elevated glucose together (OPG) resulted in both increased basal insulin secretion and impaired glucose-stimulated insulin secretion (Fig. 2a). Next, we examined insulin granules by density sedimentation in control (BSA) compared to OPG-cultured 832/3 cells. Here, we observed a significant shift of insulin-containing granules to lighter density fractions from OPG

cultured cells, suggesting there was an alteration to granule composition (Fig. 2b). Consistent with this, we observed a decrease in the expression of some granule markers, PC2 and CPE, whereas other markers, such as CgB, were unaffected (Fig. 2c, d). A similar decrease of PC2 and CPE was observed in islets from overtly diabetic C57BLKS/J db/db mice compared to non-diabetic db/+ controls (Fig. s2), which is consistent with previous reports[37]. Furthermore, fluorescent pulse-chase labeling using our proCpepSNAP reporter system revealed that OPG-cultured 832/3 cells displayed increased retention of nascent proinsulin-containing granules proximal to the Golgi (less than 3 μm) and decreased numbers of granules distal to the Golgi (greater than 5 μm; Fig. 2e, f). Additional analysis by TIRF microscopy confirmed the decrease in nascent granules reaching the plasma membrane after a 4 h chase (Fig. 2g). Following a prolonged chase (> 18 h), we observed an identical count of nascent granules between BSA (control) and OPG-cultured cells (Fig. s2c). Collectively, these data demonstrate impairments in insulin granule formation both cell culture and animal models of β-cell dysfunction and suggest that the decline in granule formation is due to a delay in proinsulin trafficking.

Proximity labeling of the proinsulin interactome reveals an ER export delay

We hypothesized that changes in the proteins interacting with proinsulin along the secretory pathway contribute to the reduced formation of insulin secretory granules. To address this, we used an *in situ* proximity labeling strategy to systematically map the proinsulin interactome via the engineered ascorbate peroxidase, APEX2, inserted within the C-peptide region of human preproinsulin (proCpepAPEX2), which is analogous to our proCpepSNAP construct. In the presence of hydrogen peroxide, APEX2 generates a short-lived (<1 ms), membrane

impermeable, biotin-phenoxy radical that biotinylates neighboring proteins *in situ* within a small labeling radius (20 nm; labeling time < 1 min) allowing us to capture transient protein interactions that are difficult to monitor with traditional approaches[38,39]. Expression of V5-tagged proCpepAPEX2 in 832/3 cells co-localized with insulin by immunostaining (Fig. 3a). Furthermore, we observed substrate-dependent (biotin-phenol and hydrogen peroxide) biotinylation of putative proinsulin-interacting proteins identified with a fluorescent streptavidin probe (Fig 3b; endogenous biotin-containing carboxylases are detected independent of APEX2 labeling). Affinity purification of proCpepAPEX2 biotinylated proteins (Fig. 3c) revealed interactions with the ER resident chaperone, GRP94, and granin protein, CgB, which have both been demonstrated to regulate proinsulin trafficking[21,25,26]. In contrast, no labeling of the plasma membrane SNARE, syntaxin-4, was observed, as expected.

Using the proximity labeling system, we identified proinsulin-interacting proteins by quantitative proteomics. We first compared peroxide (APEX2 dependent labeling) to non-peroxide (APEX2 independent labeling) treatments (Fig. s3a) and identified 74 proteins with greater than 1.2 fold enrichment, which we categorized by their subcellular locations (Fig. 3d, e). As expected, numerous ER resident chaperones (Hspa5, Hsp90b1), ER oxidoreductases (Pdia1/P4hb, Prdx4), and secretory granule proteins (CgB, Vgf) were observed to interact with proinsulin, which have all been previously demonstrated to regulate proinsulin folding[24–29] and trafficking[20,21]. We next examined changes in the proinsulin interactome in 832/3 cells cultured with elevated glucose and fatty acids (OPG) compared to control (BSA) cells (Fig. s3b-d). Analysis by subcellular location revealed a selective increase in proinsulin interactions with ER resident proteins and a corresponding decrease in interactions with proteins residing in more distal secretory

compartments (Golgi, secretory granule) (Fig. 4a, c). Enriched interactions with the majority of ER proteins, such as BiP (Hspa5) and GRP94 (Hsp90b1), occurred independent of changes in gene expression (Figs. 4b and s3e,f), whereas a subset of ER oxidoreductases, including Txndc12 and Prdx4, were modestly upregulated (Fig. 4b). Similarly, decreased interactions with various secretory proteins, such as TMED9, TMED10, and CgB, were not accompanied by changes in protein expression (Fig. 2c,d and s3e, f).

Based on our observation of increased interactions of proinsulin with ER proteins in a model of β-cell dysfunction, we hypothesized that ER export of proinsulin is delayed, which leads to impairments in insulin granule formation (Figs. 1, 2). To test this, we modified our pulse-chase labeling protocol to capture early-stage transit of proinsulin from the ER to Golgi (Fig. s1c) using GRP94 and TGN38 immunostaining to demarcate the ER and Golgi, respectively. As expected, examination of control (BSA-cultured) cells demonstrated successful trafficking of newly-synthesized proinsulin (proCpepSNAP) to the Golgi, which was largely absent from the ER (Fig. 4d, e). In contrast, pulse-chase labeling in OPG-cultured β-cells revealed a substantial retention of nascent proinsulin coincident with the ER and very little detection within the Golgi. Quantitation revealed a significant decrease in the ratio of Golgi to ER proCpepSNAP fluorescence intensity in OPG-cultured cells (Fig. 4d). To further test this, we examined proinsulin trafficking in β-cells from overtly diabetic C57BLKS-db/db mice, which displayed a profound impairment in glucose tolerance (Fig. 5a) accompanied by the loss of glucose-regulated insulin secretion (Fig. 5b). While β-cells from normoglycemic db/+ controls displayed the expected trafficking of newly synthesized proinsulin (proCpepSNAP) from the ER to the Golgi, we observed a substantial retention of nascent proinsulin within the ER in β-cells from db/db

diabetic mice (Fig. 5d) with a significant decrease in the Golgi to ER proCpepSNAP fluorescence (Fig. 5c). Importantly, the increased retention of nascent proinsulin in the ER was not accompanied by distension of the ER lumen or other changes in ER ultrastructure (Fig. 5e), consistent with previous reports in both human and rodent diabetic β-cells[11,15,40].

We further explored if activation of the ER stress response occurred in our cell culture model despite the failure to detect changes in ER ultrastructure in β-cells isolated from diabetic db/db mice (Fig. 5e). In 832/3 cells cultured with fatty acid alone (OP) or fatty acid plus elevated glucose (OPG), we failed to detect upregulation of ER stress markers, ATF4, CHOP, XBP-1(s/u), GADD34 or BiP, by qRT-PCR as compared to thapsigargin-treated cells (Fig. 6a). Similarly, expression of CHOP protein and cleaved caspase 3 were not detected under OPG culture conditions (Fig. 6b). Furthermore, pulse-chase analysis using our fluorescent proCpepSNAP reporter revealed that the chemical chaperone, TUDCA, which has been used to ameliorate ER stress[41], could not rescue the proinsulin ER export delay observed in OPG-cultured 832/3 cells (Fig. s4c).

To determine if the ER export delay was specific to proinsulin or instead was a general defect in ER protein export, we examined ER-Golgi trafficking of another granule protein, CgB, using an analogous pulse-chase system, CLIPtag. Notably, CLIPtag uses a distinct substrate from SNAPtag allowing us to perform dual pulse-chase studies of both proteins in the same cell[42]. We generated a C-terminal CLIP-tagged CgB reporter, which was expressed at levels similar to endogenous CgB (Fig. s5a) and co-trafficked with proCpepSNAP into punctate structures, likely

representing maturing insulin granules (Fig s5b). Using this dual pulse-chase system (Fig. s1d), we demonstrate that in BSA-cultured (control) 832/3 cells, nascent proinsulin (proCpepSNAP) and CgB (CgB-CLIP) similarly traffic to the Golgi following pulse-chase labeling (Fig. 6c). In OPG-cultured 832/3 cells, CgB-CLIP trafficking from the ER to Golgi occurred without delay and mirrored control (BSA) cells (Fig. 6c) with similar co-localization to the Golgi marker, TGN38 (Fig. 6e). This was in stark contrast to proinsulin, which was retained in the ER in OPG-cultured 832/3 cells (Fig. 6c), displaying reduced co-localization with both CgB-CLIP (Fig. 6d) and the Golgi marker TGN38 (Fig. 6e). Collectively, these data demonstrate a specific delay in ER export of proinsulin accompanying chronic exposure to hyperglycemic and hyperlipidemic-like conditions, which is independent of overt ER stress or a general impairment in ER protein export.

ER redox homeostasis

In hepatocytes, metabolic alterations can directly influence ER redox homeostasis via the generation of glutathione (GSH) reducing equivalents[32]. Whether a similar link exists in β-cells is not known, but alterations in ER redox poise could explain the defects in ER export of proinsulin in diabetes models. To test this, we first examined mitochondrial function in control (BSA) and OPG-cultured 832/3 cells and demonstrate a significant reduction in overall mitochondrial function (Fig. 7a), including a decrease in basal respiration (Fig. 7b), maximum respiration (Fig. 7c), and ATP production (Fig. 7d), consistent with past reports[34]. Furthermore, reduced mitochondrial metabolism coincided with a corresponding shift in the redox balance of glutathione to the oxidized state (GSSG; Fig. 7e) that was not simply due to an increase in the

production of reactive oxygen species (Fig. s6a). Because reduced glutathione (GSH) is a final electron acceptor for PDIs regulating disulfide bond isomerization[30,31], we reasoned that the decrease in GSH may preclude proinsulin disulfide bond formation leading to an ER export delay as previously suggested[29,33]. To test this, we examined if addition of chemical reducing equivalents, DTT, can rescue the proinsulin trafficking delay in OPG-cultured β-cells. Note that the concentration of DTT used was insufficient to activate the ER stress response (data not shown), did not impact β-cell function following overnight exposure in islets (Fig. s6c), but did lower the GSSG/GSH ratio (Fig. s6b). In control (BSA cultured) cells, acute addition of DTT (4 h) had no discernible impact on ER to Golgi trafficking of newly synthesized, proCpepSNAP-labeled, proinsulin (Figs. 7f, g and s6d). In contrast, acute DTT treatment restored ER to Golgi proinsulin trafficking in OPG-cultured β-cells (Fig. 7f, g). These data suggest that mitochondrial dysfunction in T2D leads to an insufficient supply of reducing equivalents necessary to maintain efficient ER export of proinsulin.

Glutathione (GSH) reducing equivalents are generated by the NADPH-dependent enzyme, glutathione reductase (Gsr1). Based on this, we reasoned that NADPH production may be necessary to support ER functions (proinsulin disulfide bond formation and export) via supplying GSH reducing equivalents. To test this, we used shRNA-mediated knockdown of the major cytosolic NADPH-producing enzyme, Idh1, which has been previously shown to support insulin granule exocytosis[35,36,43]. Note that Idh1 loss does not impair mitochondrial function[36]. Here, islets were treated with recombinant adenovirus expressing either a shRNA targeting Idh1 or a control, non-targeting shRNA, SAFE (Fig. 8). Notably, this viral backbone co-expresses mCherry from a separate RNA pol II promoter (PGK) allowing the specific identification of

transduced (Idh1 or SAFE control shRNA) islet cells[21]. Islets were co-treated with recombinant adenovirus expressing proCpepSNAP under control of the rat insulin promoter (RIP) to ensure β-cell specific transgene expression, such that mCherry+ proCpepSNAP+ cells correspond to Idh1 (or control) knockdown β-cells. Using this system, we observed strong suppression of Idh1 by qRT-PCR (Fig. 8a) and Idh1 loss did not alter total insulin content (Fig. 8b). Next, we examined insulin granule formation using pulse-chase labeling of our proCpepSNAP reporter. We observed the formation of ~400 nascent granules per control (SAFE) cell (Fig. 8c, d), consistent with our previous findings (Fig. 1e, f). In contrast, Idh1 shRNA KD β-cells, exhibited a substantial (> 50%) decrease in nascent (proCpepSNAP-labeled) insulin granules formed. Collectively, our data demonstrate that proinsulin trafficking and insulin granule formation can be regulated by NADPH production and reducing equivalent (glutathione) availability and highlight a direct link between mitochondrial and secretory dysfunction in the decline of β-cell function in T2D.

Discussion

Defects in the β-cell's secretory pathway, including changes to insulin trafficking, reduced insulin storage, impaired proinsulin processing, and hyperproinsulinemia, have been known for decades to occur in T2D[9–15]. Increased exocytosis of immature granules[16] as well as enhanced degradation of newly synthesized insulin granules in T2D[17,18] contribute to the overall decrease in insulin storage and hyperproinsulinemia; however, the underlying mechanisms for these defects are poorly understood and the links to overnutrition and hyperglycemia remain vague. Our study focuses on an emerging concept that oxidative protein folding in the ER is perturbed in the pathogenesis of β-cell dysfunction[28,29,33] and we directly link this defect to the loss of insulin granules. We show that changes in cellular redox homeostasis delay proinsulin export from the ER leading to decreased insulin granule formation in animal and cell culture models of overnutrition and diabetes. Furthermore, our data highlight a direct link between nutrient metabolism and the β-cell's secretory pathway as a critical node in the regulation of insulin biosynthesis (Fig. 9).

Following the emergence of nascent proteins from the ER protein-conducting channel, Sec61, disulfide bonds readily form in the oxidizing environment of the ER lumen. In the case of disulfides arising from non-sequential cysteine residues, such as the three disulfide bonds in proinsulin, rearrangement of mis-paired disulfides requires reduction via PDIs and subsequent re-oxidation of cysteines to form the correct disulfide linkages[27,31]. Glutathione- and thioredoxin-reducing equivalents are necessary to reset PDIs for sequential rounds of client protein disulfide bond isomerization. Here, we propose that the ER lumen becomes

hyperoxidizing during the pathogenesis of β-cell dysfunction, which impedes the necessary re-shuttling of proinsulin's disulfide linkages and thereby delays ER export of proinsulin. Using our proximity labeling system, we identified 11 ER oxidoreductases, including Prdx4 and Pdia1, that interact with proinsulin under normal, physiological conditions. Following chronic exposure to hyperglycemic and hyperlipidemic-like conditions, the increase in oxidized glutathione disulfide (GSSG) coincided with a significant elevation in the interactions between proinsulin and ER oxidoreductases as previously suggested[29]. The net result is a delay in ER export of proinsulin, which can be reversed by the addition of chemical reducing equivalents. In support of this mechanism, mis-paired intermolecular disulfide bonds between proinsulin molecules has been demonstrated in both human and rodent diabetes models[29,33] and likely requires active ERAD to alleviate proinsulin aggregates[18]. Moreover, antioxidant treatment has been shown to reduce ER stress and attenuate β-cell dysfunction and diabetes onset[44–46]. In contrast, CgB, which contains a pair of sequential cysteines forming its single disulfide linkage, is unaffected in ER to Golgi transit following nutrient stress. Together, these data provide compelling evidence linking defects in oxidative protein folding in the ER to a decrease in insulin granule formation via delayed ER export of proinsulin during the progression of β-cell dysfunction in T2D.

Numerous studies have demonstrated that induction of ER stress can perturb β-cell function and may contribute to the development of β-cell dysfunction in T2D[47]. Loss of critical ER stress response sensors, such as PERK and Ire1α, can sensitize β-cells to nutrient stresses and/or directly impair β-cell function leading to the development of diabetes[45,48–50]. Similarly, loss of the ER chaperone, GRP94, the BiP co-chaperone, $p58^{IPK}$, and PDIs, Pdia1 and Prdx4, compromise proinsulin folding, resulting in ER stress and loss of insulin content[25,26,28]. In

humans, monogenic forms of diabetes arising from *INS* mutations can prevent proper proinsulin disulfide bond formation acting as dominant negative suppressors of wild type proinsulin trafficking[51–53]. While these studies demonstrate that perturbations in ER functions and proinsulin folding can compromise β-cell health and insulin production, direct evidence for ER stress as a causative feature in the development of T2D is less clear[15,40]. Increased PERK and Ire1α activity have been described in pre-diabetic β-cells[47,54,55], yet diminished, rather than increased, expression of ATF6 and XBP-1(s) occur in β-cells from humans with long-standing T2D[54]. Human β-cells are known to cycle between varying levels of UPR protein expression[56], which may represent the natural β-cell adaptation to changes in nutrient load. Furthermore, activation of the ER stress pathway is necessary for the β-cell proliferative response to diet-induced obesity indicating that these pathways are required for normal β-cell adaptive responses[57]. Thus, it remains to be determined when modulation of the ER stress response transitions from a homeostatic adaptation of increased ER protein load to a maladaptive response that contributes to dysfunction. Expansion of ER membranes has been demonstrated in both human and rodent T2D β-cells, which may be necessary to support increased proinsulin biosynthesis[1,11,15,40]; however distension and/or dilation of the ER lumen, a classic marker of proteotoxic ER stress, is not commonly observed. Consistent with these data, we failed to detect changes in ER ultrastructure in diabetic db/db mice and saw little evidence for overt ER stress response activation in our cell culture model, despite clear effects on ER retention of proinsulin in both models. These unresolved issues encourage continued investigation in defining how physiological stresses manifest in the β-cell and determining when the adaptive responses become insufficient to mitigate cellular damage and/or become maladaptive.

Recent data demonstrates that ER protein folding can be regulated via nutrient metabolism[32]. The generation of NADPH by TCA cycle activity and subsequent production of reducing equivalents, glutathione and/or thioredoxin, by the NADPH-dependent enzymes, glutathione reductase and thioredoxin reductase, respectively, are critical to maintaining ER redox homeostasis[30,31]. Distinct from other cell types, the β-cell is uniquely positioned to sense physiological glucose fluctuations via generation of metabolic signals. The coordination of nutrient metabolism and β-cell function is well-established at multiple levels including gene expression, both transcriptionally and translationally, signaling cascades, and stimulus-coupled exocytosis[1]. Here, we speculate that nutrient metabolism is also directly coupled to β-cell secretory function through the regulation of ER redox poise to maintain insulin production (Fig. 9). Through this mechanism, chronic exposure to nutrient excess has the unfortunate consequence of impairing mitochondrial function with diminished production of NADPH and glutathione/ thioredoxin reducing equivalents necessary for ER function[34–36]. This hyperoxidizing ER lumenal environment directly impedes proinsulin trafficking and insulin granule formation leading to a diminished supply of available insulin to combat hyperglycemia. Based on this model, future studies examining the mechanisms intertwining β-cell nutrient metabolism and secretory function may offer unique insight into novel pathways that could be exploited for diabetes treatment.

Experimental Procedures

Cell culture, islet isolation, and reagents

832/3 cells (a kind gift from Dr. Christopher Newgard) were cultured as previously described[58]. For introduction of adenoviral reporters, cells were transduced with ~1-5 x 10^7 IFU/ mL adenovirus for 18 h and assayed 72-96 h post-treatment. Cell culture reagents were from Thermo Life Technologies unless specified otherwise. Chemical reagents were from Sigma-Aldrich unless specified otherwise. BSA-conjugated fatty acid solution was prepared as follows: Oleate/palmitate (2:1; 10 mM) was dissolved in water at 95^0C, cooled to 50^0C, BSA (Sigma, fatty acid free) added to a final concentration of 10%, and maintained at 37^0C for an additional 1 h. Mouse islets were isolated via collagenase V digestion and purified using Histopaque 1077 and 1119. Islets were cultured in RPMI supplemented with 10% fetal bovine serum and 1 % penicillin and streptomycin and maintained at 37°C in 5% CO_2. Pools of islets were transduced with ~1-5 x 10^8 IFU/ mL adenovirus for 18 h and assayed 72-96 h post-treatment.

Animal studies

Male C57BL6/J mice (8-10 wk old; Jackson Laboratories) were placed on a Western diet (Research Diets, D12079B) or standard chow for up to 14 weeks. Body weight and *ad lib* fed blood glucose were measured weekly. BKS.Cg-Dock7^m (C57BLKS/J) Lepr$^{db/+}$ and Lepr$^{db/db}$ mice (db/+, db/db) were either generated by heterozygous cross and genotypes confirmed via real time PCR according to Jackson Laboratories or directly purchased from Jackson Laboratories. Hyperglycemic db/db mice (*ad* lib fed blood glucose > 220 mg/dl) were compared to age-matched (10-14 weeks old), normoglycemic littermate controls (db/+). Glucose tolerance

was measured in 4-6 hr fasted mice given a 1 mg/ g body weight glucose (i.p.) challenge. Blood glucose was determined using a One Touch Ultra 2 glucometer. Plasma insulin was determined by ELISA (ALPCO). All animal protocols were approved by the University of Iowa Institutional Animal Use and Care Committee

Plasmids and viruses

The shuttle plasmid, pENTR-RIP, containing a rat insulin promoter (RIP), multiple cloning site, chloramphenicol resistance marker, ccdB, and a bovine growth hormone (bGH) polyA signal was generated by Gibson assembly (IDT) and subcloned into pENTR2b (Thermo Life) replacing the entire cassette between the attP1 and attP2 sites. V5-tagged APEX2 was inserted near the ApaI site of human preproinsulin via gblock synthesis (IDT) and subcloned into pENTR-RIP via Gibson assembly. PCR fragments of CgB (DNASU) and CLIP (gift from Eric Campeau; RRID:Addgene_29650) were subcloned into pENTR-RIP via Gibson assembly. RIP-proCpep-APEX2 and RIP-CgB-CLIP were assembled into a modified pAd-PL/DEST via Gateway cloning using LR Clonase II. Adenovirus containing rat insulin promoter (RIP) expressing Grx1-GFP2 was a kind gift from A. Linneman, Indiana University School of Medicine[59]. Recombinant adenoviruses were generated in HEK293 cells and purified by cesium chloride gradient. All sequences were verified by the Iowa Institute of Human Genetics, University of Iowa.

Glucose-stimulated insulin secretion

Insulin secretion was measured by static incubation as previously described[20]. Cells were lysed in RIPA buffer and total protein determined by BCA (Pierce). Insulin (secreted and content) was measured by ELISA (rodent 80-INSMR-CH10; ALPCO) or Alphalisa (AL204C; Perkin-Elmer Insulin).

Immunoblot analysis

Clarified cell lysates were resolved on 4-12% NuPAGE gels (Thermo Life Technologies) and transferred to supported nitrocellulose membranes (BioRad). Membranes were probed with diluted antibodies raised against chromogranin B (goat, Santa Cruz C-19 1:1000), CHOP (mouse, 1:1000 Cell Signaling 2895), cleaved Caspase 3 (rabbit, R&D systems MAB835, 1:500), CPE (rabbit, Proteintech 13710-1-AP, 1:1000), GRP94 (rabbit, kind gift of Dr. Christopher Nicchita, Duke University, 1:5000), PC2 (rabbit, Proteintech 10552-1-AP, 1:1000), proinsulin (mouse, Iowa Developmental Studies Hybridoma Bank GS-98A, 1:500), syntaxin-4 (rabbit, Millipore AB5330, 1:1000), TMED9 (rabbit, Proteintech 21620-1-AP, 1:10,000), TMED10 (rabbit, Bethyl Laboratories, A305-219A, 1:1000), gamma-tubulin (mouse, Sigma T5326, 1:10,000). Donkey anti-mouse, anti-rabbit, or anti-goat antibodies (Licor) coupled to IR-dye 680 or 800 were used to detect primary antibodies. Streptavidin-conjugated to IR dye 680 (1:1000, Thermo) was used to detect biotinylated proteins. Blots were developed using an Odyssey CLx Licor Instrument.

Fluorescence microscopy and imaging

Isolated islets expressing proCpepSNAP (AdRIP) were dispersed into monolayers using Accutase (Sigma-Aldrich) and plated onto HTB9 coated coverslips or 6 cm glass bottom dishes (Mattek) as previously described[21,60]. 832/3 cells stably expressing proCpepSNAP were plated on HTB9 coated coverslips at low density and cultured overnight as previously described[21]. For SNAPtag labeling, cells were initially incubated with SNAPcell block (10 μM; NEB) diluted in culture media for 20 min, washed 3 times for 5 min each. To allow for *de novo* protein synthesis of new proCpepSNAP, cells were cultured for an additional 2 h in experiments examining post-Golgi granule formation or 45 min in experiments examining ER-Golgi transport. Cells were pulse-labeled with SNAPcell-505 (1 μM; NEB) for 20 min in media, washed 3 times for 5 min each in culture media with reduced glucose (5 mM) and chased as indicated. For studies utilizing CgB-CLIP, an identical labeling scheme was followed using CLIPcell block (10 μM; NEB) and CLIPcell-TMR (1 μM; NEB) where appropriate. Following treatments, cells were fixed in 10 % neutral-buffered formalin. For immunostaining, cells were incubated overnight with antibodies raised against GM130 (mouse, BD Transduction 610823, 1:200), GRP94 (rabbit, kind gift of Dr. Christopher Nicchita, Duke University, 1:500), TGN38 (mouse, Novus Biologicals NB300-575, 1:200), or V5 epitope tag (rabbit, GeneTex GTX117997, 1:100) as indicated. Highly cross-adsorbed fluorescent conjugated secondary antibodies (whole IgG, donkey anti-guinea pig-AlexaFluor 488, donkey anti-rabbit rhodamine red-X, donkey anti-mouse AlexaFluor 647; Jackson ImmunoResearch) were used for detection. Cells were counterstained with DAPI and mounted using Fluorosave (Calbiochem). Images were captured on a Leica SP8 confocal microscope using a HC PL APO CS2 63x/1.40 oil objective with 3x zoom as z-stacks (5 per set, 0.3 μm step, 0.88 μm optical section) and deconvolved (Huygen's Professional). Granule distance measurements from the Golgi were determined using a distance transformation

module in Imaris (Bitplane) from spot-rendered granules (SNAP-505 labeled) and surface rendering of the Golgi identified by GM130 or TGN38 immunostaining. Granule distances were binned and expressed as a percentage of the total to normalize between cells. For islet studies, we used a cutoff of less than 0.5 μm to identify granules proximal to the Golgi as attached, and granules > 2 μm as successful Golgi export based on time course studies of granule distance clustering[21]. Golgi/ER fluorescence of SNAP labeling was determined from thresholded masks defining Golgi and ER area by immunostaining using Fiji NIH software. For plasma membrane detection, immunostained (fixed) cells were maintained in PBS and imaged using a Leica TIRF AM microscope (100x oil objective) in TIRF mode with a penetration depth of 110-150 nm. In some experiments, SNAP25 immunostaining was used to define the plasma membrane. Granule numbers from SNAP-labeling, cell area and or cell number (defined by nuclei) were determined by Fiji/ImageJ plugins.

For glutathione (GSSG/GSH) redox measurements, 832/3 cells treated with AdRIP-Grx1-GFP2 were imaged on an inverted Olympus IX83 microscope with a 20x objective (HC PL APO CS2; 0.75 NA) using Chroma 49002 GFP/CY2 Bandpass (470/535) and custom Chroma BX3-mounted (395/510) filters. Cells were subsequently cultured and re-imaged following DTT (10 mM) and diamide (5 mM) treatment, for 12 min each[43]. Fluorescent intensities of each channel were calculated from masked images (to remove background) of whole cells using Fiji NIH software. Ratiometric intensities (395 nm/470 nm) were normalized by comparing to DTT (0%) and diamide (100%) treated samples using GraphPad Prism software.

For ROS measurements, 832/3 cells were cultured in opaque HTB9-coated 96-well plates as indicated. Menadione (100 μM) treatment for 1 h was used as a positive control. Cells were incubated for 0.5 h with Cell ROX Deep Red (5 μM), washed, and analyzed using a Spectromax MD5 plate reader.

Ultrastructure

All EM related reagents were from Electron Microscopy Sciences (EMS; Hatfield, PA). Isolated islets were PBS washed and fixed in 2.5% glutaraldehyde, 4 % formaldehyde cacodylate buffer overnight (16-18 h) at 4ºC. Tissue was post-fixed in 1% OsO_4 for 1 h, dehydrated using a graded alcohol series followed by propylene oxide and embedded in Epon resin as previously described[61]. Resin blocks were cut to ultrathin (50-70 nm) sections with a diamond knife and mounted on Formvar-coated copper grids. Grids were double contrasted with 2% uranyl acetate then with lead citrate. Images were captured at 1,500x, 3,000x, 6,000x, and 8,000x magnifications by a JEOL JEM-1400 transmission electron microscope.

Density gradient isolation of secretory granules

Cells were collected, washed in ice-cold PBS, and disrupted using 15 strokes in a pre-chilled ball-bearing cell homogenizer (Isobiotec) with a 14 μm clearance in 10 mM MES pH 6.5, 1 mM MgSO4, 1 mM EDTA, 0.3 M sucrose as previously described[20,21]. Post-nuclear supernatants were layered atop 8-23% linear iodixanol (Optiprep) gradients and resolved at 110,000 x g's in an SW41 for 16-18 h. Fractions were manually collected by tube puncture. Iodixanol gradients

were verified by absorbance at 340 nm. Insulin content was determined by ELISA (ALPCO) and normalized to the total insulin content from post-nuclear supernatant.

APEX2 biotinylation and proteomics analysis

APEX2 biotinylation was performed using modified protocol[38]. Cells expressing proCpepAPEX2 were cultured for 1 h in SAB containing 2.5 mM Glc followed by addition of 500 μM biotin phenol (Adipogen) for 0.5 h. Diluted H_2O_2 was added to a final concentration of 1 mM and incubated for 1 min. Non-peroxide-treated samples were used as controls for non-enzymatic labeling such as endogenous biotin-containing proteins. Cells were washed 5x in PBS containing 10 mM sodium ascorbate, 5 mM Trolox (Acros), and 10 mM sodium azide for 1 min each. Cells were scraped, collected by centrifugation, and lysed in RIPA containing 10 mM sodium ascorbate, 5 mM Trolox, 10 mM sodium azide, and Halt protease cocktail (Thermo). For proteomics studies, cell pellets were snap frozen in a dry-ice ethanol bath prior to lysis. Pierce-660 (Thermo Life) was used to determine protein concentrations. For pulldowns, clarified cell lysates (1-2 mg/mL) were added to high capacity Neutravidin agarose resin (Thermo Life) and rotated end over end overnight (16-18 h) at 4°C. Bound proteins were washed in RIPA, 1 M KCl, 0.1 M sodium carbonate, 2 M urea in 10 mM Tris pH 8.0, RIPA solution without detergent, and eluted at 70°C for 15 min in 2x LDS sample buffer (Thermo Life) containing 2 mM biotin.

Proteomic analysis was performed on Neutravidin affinity-purified lysates (~1.5 mg starting material) with reproducible recovery verified with 4-12% NuPAGE (Thermo Life) and silver staining. Sample pre-cleaning and in-solution tryptic digestions were accomplished with a lab-

built silica / C-18 trapping mini-column[62]. Recovered peptides were labeled by reductive amination as previously described[63] using distinct (light, medium, heavy) dimethyl isotopomers[63–65]. Completion of labeling was confirmed by MALDI-TOF and distinct isotopomer-labeled samples from each treatment were mixed at equal ratios for LC–MS/MS analysis. Rather than subtracting the median ratio of spatially inaccessible false positives to normalize regional APEX, heavy (+36) and light (+28) isotopes were applied in crossover to two replicates of samples cultured in OPG vs BSA control. Non-peroxide treated (no APEX labeling) cells were labeled with the medium isotopic channel (+32). Mass spectrometry data were collected using an QExactive hf mass spectrometer coupled to an Easy-nLC-1200™ System. The autosampler typically loads 0.3ug of reconstituted digest 2.5cm C18 trap (New Objective, P/N IT100-25H002) coupled to waste or a 200cm x 75um pillar array column from PharmaFluidics. The column floated at high voltage via a gold connector secured to the micro-cross assembly (IDEX, P/N UH-752). MS1 scans were acquired every 3 sec. with automatic gain control set to 3e05 and 60,000 resolution. Ions with 2 to 6 charges were isolated within a 1.2 Th pass window and targeted for HCD activation. The AGC target for HCD was 41.2E05, 30% NCE, using 75 ms maximum fill time. and 30k resolution at 400 m/z. Searches were performed with both MaxQuant, version 1.6.11 and Byonic search engines (Protein Metrics ver. 2.8.2). Search databases were composed of the Uniprot KB for rat. Searches were set to accept static ReDi labels and +57 on Cys residues. Variable oxidation was assumed to occur at Met only. Quantification was achieved by comparing the integrated intensity of each MS1 channel in a sequence-matched triplet derived from the multiplexed sample. Scaffold was used to collate fold enrichment of BSA- and oleate/palmitate + glucose-cultured samples compared to non-peroxide-treated samples. Classifiers to assign active engagement in ISG assembly were

established by ROC curve analysis as described[38]. The $\log_2$ threshold fold change of 1.2 or greater enrichment in the BSA (control) cultured samples relative to no peroxide control was determined. For proteins with a $\log_2$ fold change of 1.2 or greater enrichment in the BSA (control) cultured samples, the relative fold change to oleate/palmitate + glucose cultured samples was determined. Protein subcellular locations were determined using annotations from the rat and human orthologs in the UniProt database and additional confirmation by literature searches as needed.

Metabolic studies

Mitochondrial function was evaluated using Agilent Seahorse XF96 Extracellular Flux Analyzer. 832/3 cells were seeded at a density of 40,000 cells/well in XF 96-well microplates. Cells were cultured for 72 h in BSA (control) or OPG media as indicated. Prior to the assay, cells were washed and incubated in serum-free assay medium (Dulbecco's modified Eagle's medium (DMEM) supplemented with 5mM HEPES, 2 mM L-glutamine and 1 mM Na pyruvate (Life Technologies), pH 7.40 with either 2 mM or 20 mM glucose. Mitochondrial stress tests were initiated then cellular respiration was followed by monitoring the Oxygen Consumption Rate (OCR). A basal rate was established, followed by addition of 2.5 μM Oligomycin A, 1.25 μM FCCP, and 2 μM Rotenone and Antimycin, each as sequential injections. Data were normalized following post-experiment cell enumeration.

Quantitative RT-PCR

RNA was harvested using a Zymo RNA minikit. and cDNA synthesized in an iScript reaction (Bio Rad). Real-time PCRs were performed using the ABI 7700 sequence detection system and software (Applied Biosystems). All primer sequences are available upon request.

Statistical Analysis

Data are presented as the mean ± S.E.M. For statistical significance determinations, data were analyzed by the two-tailed unpaired, Student's t test or by ANOVA with post-hoc analysis for multiple group comparisons as indicated (GraphPad Prism). A p-value < 0.05 was considered significant.

Acknowledgements

We would like to acknowledge the use of the University of Iowa Central Microscopy Research Facility, University of Iowa Proteomics Facility, and University of Iowa Radiation and Free Radical Research Core. This work was supported by startup funds provided by the Fraternal Order of Eagles Diabetes Research Center, University of Iowa to S.B.S., Department of Defense CDMRP grant PR190353 to S.B.S., National Institutes of Health grant R35GM130331to Y.W., and a National Institutes of Health Predoctoral Training Grant T32GM008629, PI Daniel Eberl to K.E.R. University of Iowa Electron Spin Resonance (ESR) Facility, Holden Comprehensive Cancer Center, is supported by NCI P30 CA086862.

Competing Interests

No competing interests declared.

Abbreviations

Biotin phenol (BP); dithiothreitol (DTT); glucose (Glc); glucose-stimulated insulin secretion (GSIS); infectious units (IFU); oleate/palmitate (OP); oleate/palmitate + Glc (OPG); protein disulfide isomerase (PDI); rat insulin promoter (RIP); Type 2 diabetes (T2D); untranslated region (UTR)

Data Availability

The datasets generated during and/or analyzed during the current study are available from the corresponding author upon reasonable request. The mass spectrometry proteomics data have been deposited to the ProteomeXchange Consortium via the PRIDE[66] partner repository with the dataset identifier PXD028606.

Figure legends

Figure 1. Insulin granule formation is impaired in rodent models of islet dysfunction. 8-10 week old male C57BL6/J mice (n=5-9) were placed on a standard chow (SC) or Western diet (WD) for 8 weeks. Body weight (**a**) and *ad lib* fed blood glucose (**b**) were recorded weekly. 4 h fasted mice were injected i.p. with 1 mg/g bw glucose and blood glucose monitored for 2 h as indicated (**c**) and plasma sampled for insulin (**d**). (**e-i**) Mouse islets (SC vs. WD C57BL6/J) were treated with AdRIP-proCpepSNAP. 48 h post-infection, islets were pulse-labeled with SNAP-505 for 20 min (green), chased for 2 h, immunostained for GM130 (magenta), and counterstained with DAPI (blue). (**e**) Representative images are shown from SC vs. WD pulse-chase labeling (scale bar = 5 μm). (**f**) Total number of nascent granules per cell are shown (n=4; 22-25 cells per mouse). (**g**) Frequency distribution of binned granule distances (microns) from the Golgi are shown per mouse (n=4). (**h-i**) C57BL6/J mice (n=5) were placed on SC or WD for 14 weeks. (**h**) Representative images captured in TIRF mode are shown from SC vs. WD pulse-chase labeling following nascent granule trafficking to the plasma membrane (scale bar = 5 μm). (**i**) The total number of plasma membrane-bound insulin granules per cell per mouse are shown (n=5-7; 26-57 cells per mouse). (**a-d, f-g, i**) Data represent the mean ± S.E.M. * $p < 0.05$ by two-way ANOVA with Sidak post-test analysis.

Figure 2. Elevated glucose and fatty acid culture impaired β-cell function and proinsulin trafficking in 832/3 cells. (**a-d**) 832/3 cells were cultured for 72 h in control media supplemented with BSA, media containing oleate:palmitate (2:1, 1mM OP), or media containing oleate/palmitate (2:1, 1 mM) and elevated glucose (20mM; OPG) as indicated. (**a**) Glucose-

stimulated insulin secretion was measured by static incubation in media containing 2.5 mM Glc followed by 12 mM Glc for 1 h each. (**b**) Cell lysates were resolved on 8-23% iodixanol gradients. Solid line represents insulin as determined by ELISA from gradient fractions; dotted line represents gradient density (absorbance at 340 nm). Representative immunoblots from whole-cell lysates were probed with CgB, PC2, and CPE antibodies are shown (**c**) and relative protein expression was quantified (**d**). (**e-g**) 832/3 cells stably expressing proCpepSNAP were cultured for 72 h in control media (BSA) or OPG as indicated. Cells were pulse-labeled with SNAP-505 for 20 min (green), chased for 2 h, immunostained for TGN38 (magenta) and counterstained with DAPI (blue). Representative images (**e**) and frequency distribution of binned granule distance (microns) from the Golgi (**f**) are shown (n=6; 35-37 cells per group; scale bar = 5 μm). (**g**) The total number of nascent (proCpepSNAP-labeled) insulin granules bound to the plasma membrane via TIRF microscopy after a 4 h chase are shown and normalized to cell area (n=3; 4 images per condition). (**a,d,f-g**) Data represent the mean ± S.E.M. *,# $p < 0.05$ by two-way ANOVA with Sidak post-test analysis.

Figure 3. APEX2 labeling reveals proinsulin interactions throughout the secretory system. (**a**) 832/3 cells expressing proCpepAPEX2 were immunostained for insulin (green), V5 (proCpepV5APEX2, red), TGN38 (magenta), and counterstained with DAPI (blue). Scale bar = 5 μm. (**b**) proCpepAPEX2 expressing 832/3 cells were treated with biotin-phenol (BP) and H_2O_2 as indicated. Cell lysates were analyzed by Western blots probed with fluorescent streptavidin or proinsulin antibody. (**c**) Lysates from proCpepAPEX2-biotinylated cells were enriched using Neutravidin agarose resin and various stages of purification analyzed by immunoblot probed with GRP94, CgB, and Syntaxin-4. (**d**, **e**) Neutravidin agarose purified proteins from

proCpepAPEX2 expressing 832/3 cells treated with or without H_2O_2 were identified by quantitative proteomics (n=4). Proteins enriched 1.2-fold or greater in peroxide-treated compared to non-peroxide-treated samples are displayed by mean-$\log_2$-fold enrichment as a function of subcellular location (**d**) or as a heatmap to visualize the changes of individual proteins (**e**).

Figure 4. Increased proinsulin interactions with ER resident proteins in 832/3 cells cultured with elevated glucose and fatty acids. 832/3 cells expressing proCpepAPEX2 were cultured for up to 72 h in control media supplemented with BSA or media containing oleate/palmitate (2:1, 1 mM) and elevated glucose (20 mM; OPG). (**a,c**) Neutravidin agarose purified proteins were identified by quantitative proteomics. Proteins enriched 1.2-fold or greater in BSA (control) cultured cells compared to non-peroxide treated samples were further analyzed as the mean (n=4) of the relative fold ($\log_2$) change of OPG compared to BSA cultured cells. Data are displayed as a function of subcellular location for individual proteins (**a**) and as a heatmap (**c**). (**b**) mRNA expression levels were determined by qRT-PCR (n=3). (**d-e**) 832/3 cells stably expressing proCpepSNAP were cultured for 72 h in BSA or OPG media as indicated. Cells were pulse-labeled with SNAP-505 for 20 min (green) then fixed and immunostained for GRP94 (red), TGN38 (magenta), and counterstained with DAPI (blue). The ratio of proCpepSNAP (green) fluorescence coincident with the Golgi (magenta) compared to ER (red) were quantified (**d**, n=6-8; 48-64 cells per condition). (**e**) Representative images are shown (scale bar = 5 μm). (**b**, **d**) Data represent the mean ± S.E.M. * $p < 0.05$ by two-way ANOVA with Sidak post-test analysis.

Figure 5. Delayed ER export of proinsulin in diabetic db/db β-cells. (**a-b**) 10-14 week old C57BLKS/J db/+ and db/db mice (n=4-5) were fasted for 4 h, injected i.p. 1mg/g bw glucose. Blood glucose was monitored for 2 h as indicated (**a**) and plasma was sampled for insulin (**b**). (**c-d**) Isolated mouse islets (C57BLKS/J db/+ vs. db/db) were treated with AdRIP-proCpepSNAP. 48 h post-infection, islets were pulse-labeled with SNAP-505 for 20 min (green), chased for 10 min, immunostained for GM130 (magenta), and counterstained with DAPI (blue). The ratio of proCpepSNAP (green) fluorescence coincident with the Golgi (magenta) compared to ER (red) were quantified (**c**, n=4; 6-36 cells per mouse). (**d**) Representative images are shown (scale bar = 3 μM). (**e**) Islets isolated from C57BLKS/J db/+ vs. db/db were examined for ultrastructure by electron microscopy. Representative micrographs depicting the ER are shown. (**a-c**) Data represent the mean ± S.E.M. * $p < 0.05$ by two-way ANOVA with Sidak post-test analysis.

Figure 6. Delayed ER export of proinsulin, but not CgB. (**a-b**) 832/3 cells were cultured for 72 h in control media supplemented with BSA, media containing oleate:palmitate (2:1, 1 mM OP) or media containing oleate:palmitate (2:1, 1 mM) and elevated glucose (20 mM; OPG) as indicated. Cells were treated for 18 h with thapsigargin (50 nM) as indicated. (**a**) mRNA expression was examined by qRT-PCR to (n=4-6). (**b**) Representative immunoblots of cell lysates. (**c-e**) 832/3 cells stably expressing proCpepSNAP were treated with AdRIP-CgB-CLIP and cultured for 72 h in BSA or OPG media as indicated. Cells were pulse-labeled with SNAP-505 (green) and CLIP-TMR (red) for 20 min, fixed and immunostained for TGN38 (magenta), and counterstained with DAPI (blue). (**c**) Representative images are shown (scale bar = 5 μm). Mander's correlation coefficient (MCC) was used to determine colocalization of labeled proCpepSNAP (SNAP) with CgB-CLIP (CLIP) (**d**) or TGN38 (**e**) or CgB-CLIP (CLIP) with

TGN38 (**e**) as indicated (n=3; 53-70 cells per condition). (**a, d-e**) Data represent the mean ± S.E.M. * $p < 0.05$ by two-way ANOVA with Sidak post-test analysis.

Figure 7. Proinsulin ER export delay can be rescued by chemical reducing agent. 832/3 cells (**a-e**) and 832/3 cells stably expressing proCpepSNAP (**f, g**) were cultured for 72 h in control media supplemented with BSA (1%) or media containing oleate/palmitate (2:1, 1 mM) and elevated glucose (20 mM; OPG) as indicated. (**a-d**) Oxygen consumption rate (OCR) was measured at stimulatory glucose (20 mM) conditions at rest and following addition of 2.5 µM oligomycin, 1.25 µM FCCP, and 2 µM rotenone + antimycin A. Overall mitochondrial function was examined (**a**) as well as basal respiration (**b**), maximum respiration (**c**), and ATP production (**d**) (n=3, up to 15 replicates per condition). (**e**) 832/3 cells treated with AdRIP-Grx1-roGFP2 were imaged at 470/535 nm and 395/510 nm and re-imaged following DTT (10 mM) and diamide (5 mM) treatment for 12 minutes each (n=5). Ratiometric intensities were normalized to DTT (0%) and diamide (100%). (**f, g**) 832/3 cells stably expressing proCpepSNAP were treated with DTT (0.5 mM) for 4 h prior to being pulse-labeled with SNAP-505 for 20 min (green), fixed, and immunostained for TGN38 (magenta), and counterstained with DAPI (blue). (**f**) Manders' correlation coefficient was used to determine the colocalization of labeled proCpepSNAP (SNAP) with TGN38 (magenta) (n=4; 71-91 cells per condition). (**g**) Representative images are shown (scale bar = 5 µm). (**a-f**) Data represent the mean ± S.E.M. * $p < 0.05$ by two-way ANOVA with Sidak post-test analysis.

Figure 8. Knockdown of mitochondrial NADPH-producing enzyme IDH1 impairs insulin granule formation. Mouse islets were treated with Ad-shRNA-SAFE (control) or Ad-shRNA-Idh1 for up to 72 h. (**a**) mRNA expression of Idh1 was determined by qRT-PCR (n=4). (**b**) Insulin content was measured from whole cell lysate per 40 islets (n=5) and mRNA expression verified by qRT-PCR. (**c-d**) Mouse islets were treated with AdRIP-proCpep-SNAP and either Ad-shRNA-SAFE or Ad-shRNA-Idh1 as indicated. 48 h post-infection, islets were pulse-labeled with SNAP-505 for 20 min (green), chased for 2 h, immunostained for GM130 (magenta), and counterstained with DAPI (blue). mCherry expression was used to identify infected cells in each condition for quantification. (**c**) Total number of nascent granules per cell are shown (n=4; 4-11 cells per mouse). (**d**) Representative images are shown from pulse-chase labeling (scale bar = 3 μm).

Figure 9. Model of metabolism-coupled proinsulin trafficking. In this model, glucose metabolism by the mitochondria generates NADPH, which is used to regulate glutathione cycling (GSH/GSSG) and produce GSH reducing equivalents. GSH is necessary to maintain sequential rounds of protein disulfide bond isomerization (RSH, RSSR) in the ER to facilitate proinsulin folding. Properly folded proinsulin can be exported from the ER to the Golgi, where it is packaged along with other proteins, such as CgB, into immature secretory granules. This model was created with Biorender.com.

Literature Cited

1. Boland, B. B., Rhodes, C. J. & Grimsby, J. S. The dynamic plasticity of insulin production in β-cells. *Mol Metab* **6**, 958–973 (2017).

2. Henquin, J. C. Regulation of insulin secretion: a matter of phase control and amplitude modulation. *Diabetologia* **52**, 739–751 (2009).

3. Henquin, J. C., Ishiyama, N., Nenquin, M., Ravier, M. A. & Jonas, J. C. Signals and pools underlying biphasic insulin secretion. *Diabetes* **51 Suppl 1**, S60-7 (2002).

4. Gembal, M., Gilon, P. & Henquin, J. C. Evidence that glucose can control insulin release independently from its action on ATP-sensitive K+ channels in mouse B cells. *J Clin Invest* **89**, 1288–1295 (1992).

5. Wicksteed, B., Alarcon, C., Briaud, I., Lingohr, M. K. & Rhodes, C. J. Glucose-induced translational control of proinsulin biosynthesis is proportional to preproinsulin mRNA levels in islet beta-cells but not regulated via a positive feedback of secreted insulin. *J Biol Chem* **278**, 42080–42090 (2003).

6. Guest, P. C., Rhodes, C. J. & Hutton, J. C. Regulation of the biosynthesis of insulin-secretory-granule proteins. Co-ordinate translational control is exerted on some, but not all, granule matrix constituents. *Biochem J* **257**, 431–7 (1989).

7. Uchizono, Y., Alarcón, C., Wicksteed, B. L., Marsh, B. J. & Rhodes, C. J. The balance between proinsulin biosynthesis and insulin secretion: where can imbalance lead? *Diabetes Obes Metab* **9 Suppl 2**, 56–66 (2007).

8. Boland, B. B. *et al.* β-Cell Control of Insulin Production During Starvation-Refeeding in Male Rats. *Endocrinology* **159**, 895–906 (2018).

9. Halban, P. A. *et al.* beta-cell failure in type 2 diabetes: postulated mechanisms and prospects for prevention and treatment. *Diabetes Care* **37**, 1751–8 (2014).

10. Kahn, S. E., Zraika, S., Utzschneider, K. M. & Hull, R. L. The beta cell lesion in type 2 diabetes: there has to be a primary functional abnormality. *Diabetologia* **52**, 1003–12 (2009).

11. Masini, M. *et al.* Ultrastructural morphometric analysis of insulin secretory granules in human type 2 diabetes. *Acta Diabetol* **49 Suppl 1**, S247-252 (2012).

12. Like, A. A. & Chick, W. L. Studies in the diabetic mutant mouse. II. Electron microscopy of pancreatic islets. *Diabetologia* **6**, 216–242 (1970).

13. Kahn, S. E. & Halban, P. A. Release of incompletely processed proinsulin is the cause of the disproportionate proinsulinemia of NIDDM. *Diabetes* **46**, 1725–32 (1997).

14. Ward, W. K., Bolgiano, D. C., McKnight, B., Halter, J. B. & Porte, D. Diminished B cell secretory capacity in patients with noninsulin-dependent diabetes mellitus. *J Clin Invest* **74**, 1318–28 (1984).

15. Alarcon, C. *et al.* Pancreatic β-Cell Adaptive Plasticity in Obesity Increases Insulin Production but Adversely Affects Secretory Function. *Diabetes* **65**, 438–450 (2016).

16. Rhodes, C. J. & Alarcon, C. What beta-cell defect could lead to hyperproinsulinemia in NIDDM? Some clues from recent advances made in understanding the proinsulin-processing mechanism. *Diabetes* **43**, 511–7 (1994).

17. Pasquier, A. *et al.* Lysosomal degradation of newly formed insulin granules contributes to β cell failure in diabetes. *Nat Commun* **10**, 3312 (2019).

18. Shrestha, N. *et al.* Sel1L-Hrd1 ER-associated degradation maintains β cell identity via TGF-β signaling. *J Clin Invest* **130**, 3499–3510 (2020).

19. Muller, A. *et al.* A Global Approach for Quantitative Super Resolution and Electron Microscopy on Cryo and Epoxy Sections Using Self-labeling Protein Tags. *Sci Rep* **7**, 23 (2017).

20. Stephens, S. B. *et al.* The Prohormone VGF Regulates beta Cell Function via Insulin Secretory Granule Biogenesis. *Cell Rep* **20**, 2480–2489 (2017).

21. Bearrows, S. C. *et al.* Chromogranin B regulates early stage insulin granule trafficking from the Golgi in pancreatic islet beta-cells. *J Cell Sci* (2019) doi:10.1242/jcs.231373.

22. Cao, M. *et al.* PICK1 and ICA69 control insulin granule trafficking and their deficiencies lead to impaired glucose tolerance. *PLoS Biol* **11**, e1001541 (2013).

23. Gandasi, N. R. *et al.* Glucose-Dependent Granule Docking Limits Insulin Secretion and Is Decreased in Human Type 2 Diabetes. *Cell Metab* **27**, 470-478 e4 (2018).

24. Arunagiri, A. *et al.* Misfolded proinsulin in the endoplasmic reticulum during development of beta cell failure in diabetes. *Ann N Y Acad Sci* **1418**, 5–19 (2018).

25. Kim, D.-S. *et al.* GRP94 Is an Essential Regulator of Pancreatic β-Cell Development, Mass, and Function in Male Mice. *Endocrinology* **159**, 1062–1073 (2018).

26. Ghiasi, S. M. *et al.* Endoplasmic Reticulum Chaperone Glucose-Regulated Protein 94 Is Essential for Proinsulin Handling. *Diabetes* **68**, 747–760 (2019).

27. Winter, J., Klappa, P., Freedman, R. B., Lilie, H. & Rudolph, R. Catalytic activity and chaperone function of human protein-disulfide isomerase are required for the efficient refolding of proinsulin. *J Biol Chem* **277**, 310–317 (2002).

28. Jang, I. *et al.* PDIA1/P4HB is required for efficient proinsulin maturation and ß cell health in response to diet induced obesity. *Elife* **8**, e44528 (2019).

29. Tran, D. T. *et al.* Unbiased Profiling of the Human Proinsulin Biosynthetic Interaction Network Reveals a Role for Peroxiredoxin 4 in Proinsulin Folding. *Diabetes* **69**, 1723–1734 (2020).

30. Birk, J. *et al.* Endoplasmic reticulum: reduced and oxidized glutathione revisited. *J Cell Sci* **126**, 1604–1617 (2013).

31. Ellgaard, L., Sevier, C. S. & Bulleid, N. J. How Are Proteins Reduced in the Endoplasmic Reticulum? *Trends Biochem Sci* **43**, 32–43 (2018).

32. Gansemer, E. R. *et al.* NADPH and Glutathione Redox Link TCA Cycle Activity to Endoplasmic Reticulum Homeostasis. *iScience* **23**, 101116 (2020).

33. Arunagiri, A. *et al.* Proinsulin misfolding is an early event in the progression to type 2 diabetes. *Elife* **8**, e44532 (2019).

34. Haythorne, E. *et al.* Diabetes causes marked inhibition of mitochondrial metabolism in pancreatic β-cells. *Nat Commun* **10**, 2474 (2019).

35. Ferdaoussi, M. *et al.* Isocitrate-to-SENP1 signaling amplifies insulin secretion and rescues dysfunctional β cells. *J Clin Invest* **125**, 3847–3860 (2015).

36. Ronnebaum, S. M. *et al.* A pyruvate cycling pathway involving cytosolic NADP-dependent isocitrate dehydrogenase regulates glucose-stimulated insulin secretion. *J Biol Chem* **281**, 30593–602 (2006).

37. Kang, T. *et al.* Proteomic Analysis of Restored Insulin Production and Trafficking in Obese Diabetic Mouse Pancreatic Islets Following Euglycemia. *J Proteome Res* **18**, 3245–3258 (2019).

38. Hung, V. *et al.* Spatially resolved proteomic mapping in living cells with the engineered peroxidase APEX2. *Nat Protoc* **11**, 456–75 (2016).

39. Lam, S. S. *et al.* Directed evolution of APEX2 for electron microscopy and proximity labeling. *Nat Methods* **12**, 51–4 (2015).

40. Marchetti, P. *et al.* The endoplasmic reticulum in pancreatic beta cells of type 2 diabetes patients. *Diabetologia* **50**, 2486–2494 (2007).

41. Ozcan, U. *et al.* Chemical chaperones reduce ER stress and restore glucose homeostasis in a mouse model of type 2 diabetes. *Science* **313**, 1137–1140 (2006).

42. Gautier, A. *et al.* An engineered protein tag for multiprotein labeling in living cells. *Chem Biol* **15**, 128–36 (2008).

43. Bauchle, C. J. *et al.* Mitochondrial Efflux of Citrate and Isocitrate Is Fully Dispensable for Glucose-Stimulated Insulin Secretion and Pancreatic Islet β-Cell Function. *Diabetes* db210037 (2021) doi:10.2337/db21-0037.

44. Malhotra, J. D. *et al.* Antioxidants reduce endoplasmic reticulum stress and improve protein secretion. *Proc Natl Acad Sci U S A* **105**, 18525–18530 (2008).

45. Hassler, J. R. *et al.* The IRE1α/XBP1s Pathway Is Essential for the Glucose Response and Protection of β Cells. *PLoS Biol* **13**, e1002277 (2015).

46. Han, J. *et al.* Antioxidants Complement the Requirement for Protein Chaperone Function to Maintain β-Cell Function and Glucose Homeostasis. *Diabetes* **64**, 2892–2904 (2015).

47. Yong, J., Johnson, J. D., Arvan, P., Han, J. & Kaufman, R. J. Therapeutic opportunities for pancreatic β-cell ER stress in diabetes mellitus. *Nat Rev Endocrinol* **17**, 455–467 (2021).

48. Harding, H. P. *et al.* Diabetes mellitus and exocrine pancreatic dysfunction in perk-/- mice reveals a role for translational control in secretory cell survival. *Mol Cell* **7**, 1153–1163 (2001).

49. Xu, T. *et al.* The IRE1α-XBP1 pathway regulates metabolic stress-induced compensatory proliferation of pancreatic β-cells. *Cell Res* **24**, 1137–1140 (2014).

50. Delépine, M. *et al.* EIF2AK3, encoding translation initiation factor 2-alpha kinase 3, is mutated in patients with Wolcott-Rallison syndrome. *Nat Genet* **25**, 406–409 (2000).

51. Liu, M., Hodish, I., Rhodes, C. J. & Arvan, P. Proinsulin maturation, misfolding, and proteotoxicity. *Proc Natl Acad Sci U S A* **104**, 15841–6 (2007).

52. Støy, J. *et al.* Clinical and molecular genetics of neonatal diabetes due to mutations in the insulin gene. *Rev Endocr Metab Disord* **11**, 205–215 (2010).

53. Haataja, L. *et al.* Distinct states of proinsulin misfolding in MIDY. *Cell Mol Life Sci* **78**, 6017–6031 (2021).

54. Engin, F., Nguyen, T., Yermalovich, A. & Hotamisligil, G. S. Aberrant islet unfolded protein response in type 2 diabetes. *Sci Rep* **4**, 4054 (2014).

55. Lipson, K. L. *et al.* Regulation of insulin biosynthesis in pancreatic beta cells by an endoplasmic reticulum-resident protein kinase IRE1. *Cell Metab* **4**, 245–254 (2006).

56. Xin, Y. *et al.* Pseudotime Ordering of Single Human β-Cells Reveals States of Insulin Production and Unfolded Protein Response. *Diabetes* **67**, 1783–1794 (2018).

57. Sharma, R. B. *et al.* Insulin demand regulates β cell number via the unfolded protein response. *J Clin Invest* **125**, 3831–3846 (2015).

58. Hohmeier, H. E. *et al.* Isolation of INS-1-derived cell lines with robust ATP-sensitive K+ channel-dependent and -independent glucose-stimulated insulin secretion. *Diabetes* **49**, 424–30 (2000).

59. Reissaus, C. A. *et al.* A Versatile, Portable Intravital Microscopy Platform for Studying Beta-cell Biology In Vivo. *Sci Rep* **9**, 8449 (2019).

60. Hayes, H. L. *et al.* Delayed apoptosis allows islet beta-cells to implement an autophagic mechanism to promote cell survival. *PLoS One* **12**, e0172567 (2017).

61. Joshi, G., Chi, Y., Huang, Z. & Wang, Y. Aβ-induced Golgi fragmentation in Alzheimer's disease enhances Aβ production. *Proc Natl Acad Sci U S A* **111**, E1230-1239 (2014).

62. Zougman, A., Selby, P. J. & Banks, R. E. Suspension trapping (STrap) sample preparation method for bottom-up proteomics analysis. *Proteomics* **14**, 1006–1000 (2014).

63. Yu, C. L. *et al.* Rapid Proteomics to Prospect and Validate Novel Bacterial Metabolism Induced by Environmental Burden. *Methods Enzymol* **586**, 379–411 (2017).

64. Boersema, P. J., Raijmakers, R., Lemeer, S., Mohammed, S. & Heck, A. J. Multiplex peptide stable isotope dimethyl labeling for quantitative proteomics. *Nat Protoc* **4**, 484–94 (2009).

65. Hsu, J.-L., Huang, S.-Y., Chow, N.-H. & Chen, S.-H. Stable-isotope dimethyl labeling for quantitative proteomics. *Anal Chem* **75**, 6843–6852 (2003).

66. Perez-Riverol, Y. *et al.* The PRIDE database and related tools and resources in 2019: improving support for quantification data. *Nucleic Acids Res* **47**, D442–D450 (2019).

Figure 1.

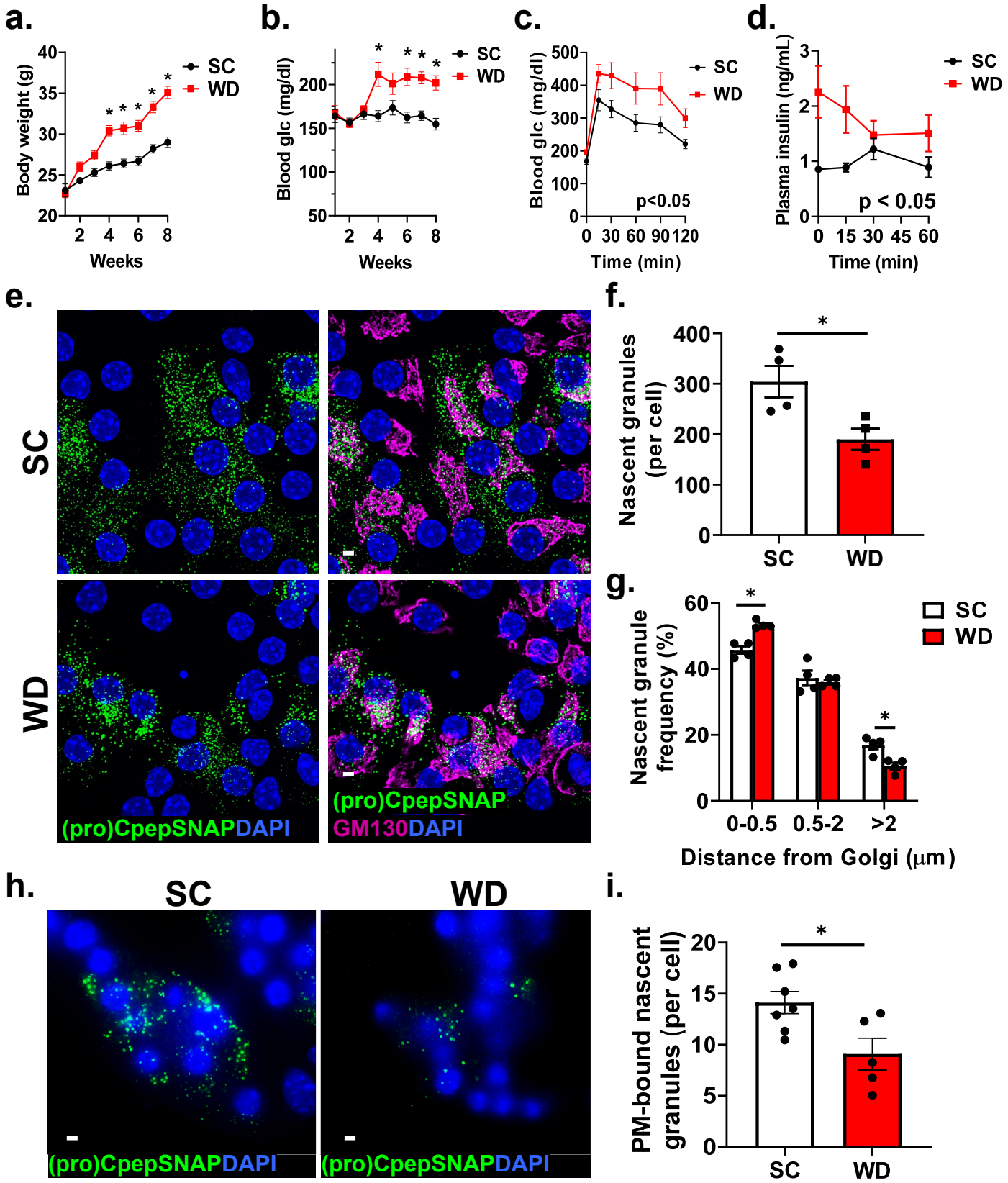
a.
Body weight (g)
Weeks
SC
WD
b.
Blood glc (mg/dl)
Weeks
SC
WD
c.
Blood glc (mg/dl)
Time (min)
SC
WD
p<0.05
d.
Plasma insulin (ng/mL)
Time (min)
SC
WD
p < 0.05
e.
SC
WD
(pro)CpepSNAPDAPI
(pro)CpepSNAP
GM130DAPI
f.
Nascent granules (per cell)
SC
WD
g.
Nascent granule frequency (%)
SC
WD
0-0.5
0.5-2
>2
Distance from Golgi (μm)
h.
SC
WD
(pro)CpepSNAPDAPI
(pro)CpepSNAPDAPI
i.
PM-bound nascent granules (per cell)
SC
WD

Figure 2.

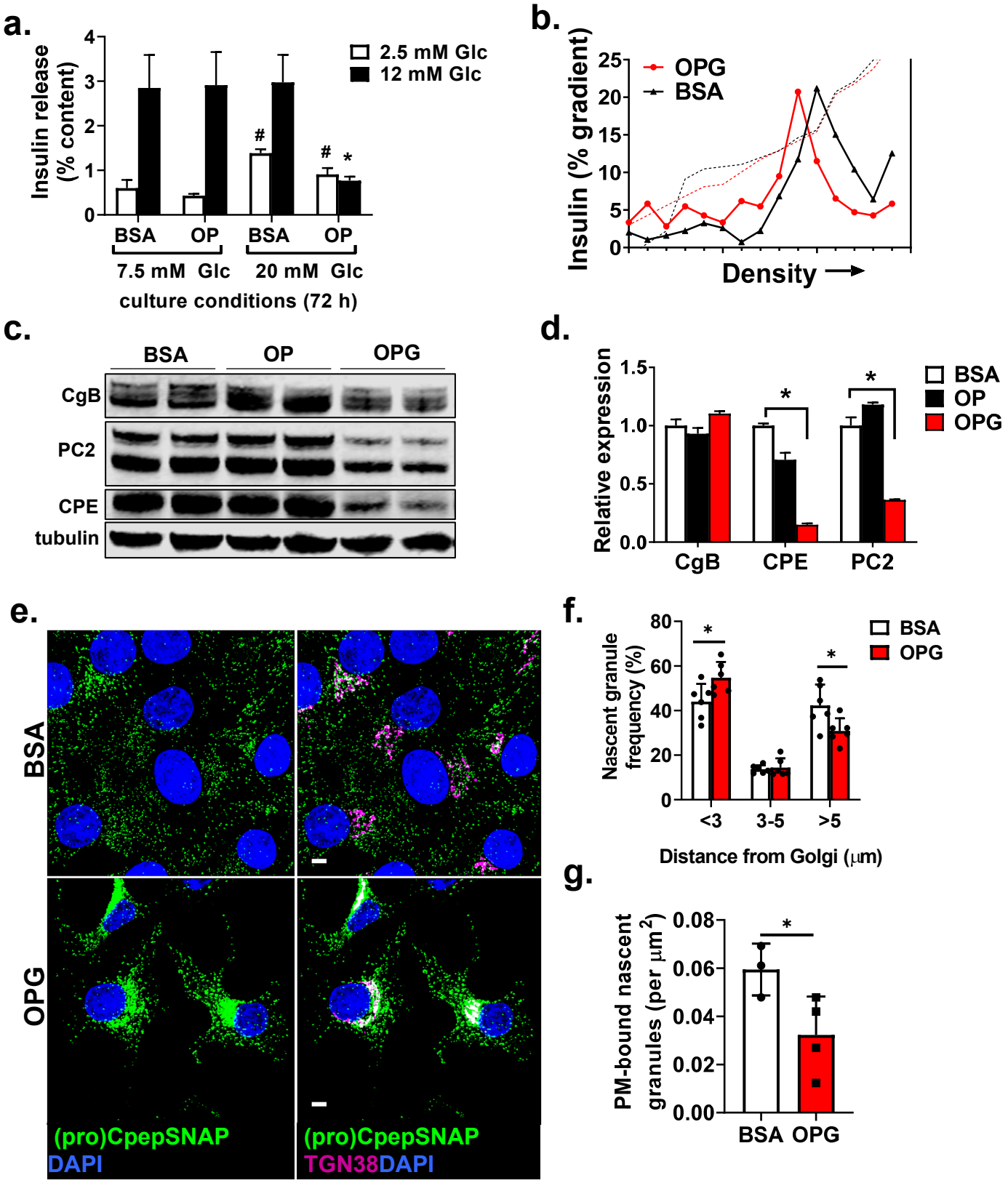
a.
Insulin release (% content)
2.5 mM Glc
12 mM Glc
BSA
OP
BSA
OP
7.5 mM Glc
20 mM Glc
culture conditions (72 h)
b.
Insulin (% gradient)
OPG
BSA
Density
c.
BSA
OP
OPG
CgB
PC2
CPE
tubulin
d.
Relative expression
BSA
OP
OPG
CgB
CPE
PC2
e.
BSA
OPG
(pro)CpepSNAP
DAPI
(pro)CpepSNAP
TGN38DAPI
f.
Nascent granule frequency (%)
BSA
OPG
<3
3-5
>5
Distance from Golgi (μm)
g.
PM-bound nascent granules (per μm2)
BSA
OPG

Figure 3.

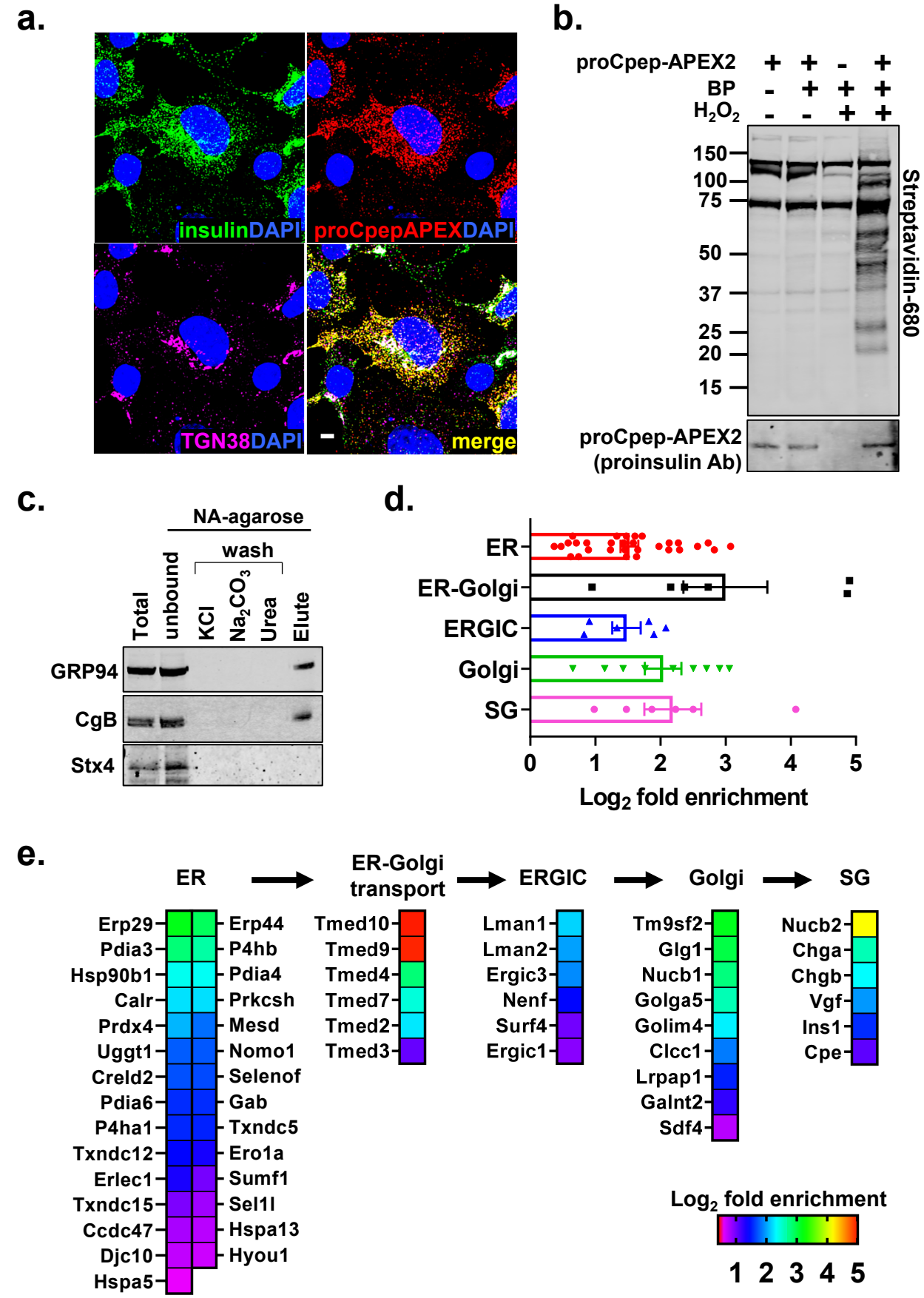
a.
insulinDAPI
proCpepAPEXDAPI
TGN38DAPI
merge
b.
proCpep-APEX2 + + - +
BP - + + +
H2O2 - - + +
150
100
75
50
37
25
20
15
Streptavidin-680
proCpep-APEX2
(proinsulin Ab)
c.
NA-agarose
wash
Total
unbound
KCl
Na2CO3
Urea
Elute
GRP94
CgB
Stx4
d.
ER
ER-Golgi
ERGIC
Golgi
SG
0
1
2
3
4
5
Log2 fold enrichment
e.
ER
ER-Golgi transport
ERGIC
Golgi
SG
Erp29
Pdia3
Hsp90b1
Calr
Prdx4
Uggt1
Creld2
Pdia6
P4ha1
Txndc12
Erlec1
Txndc15
Ccdc47
Djc10
Hspa5
Erp44
P4hb
Pdia4
Prkcsh
Mesd
Nomo1
Selenof
Gab
Txndc5
Ero1a
Sumf1
Sel1l
Hspa13
Hyou1
Tmed10
Tmed9
Tmed4
Tmed7
Tmed2
Tmed3
Lman1
Lman2
Ergic3
Nenf
Surf4
Ergic1
Tm9sf2
Glg1
Nucb1
Golga5
Golim4
Clcc1
Lrpap1
Galnt2
Sdf4
Nucb2
Chga
Chgb
Vgf
Ins1
Cpe
Log2 fold enrichment
1 2 3 4 5

Figure 4.

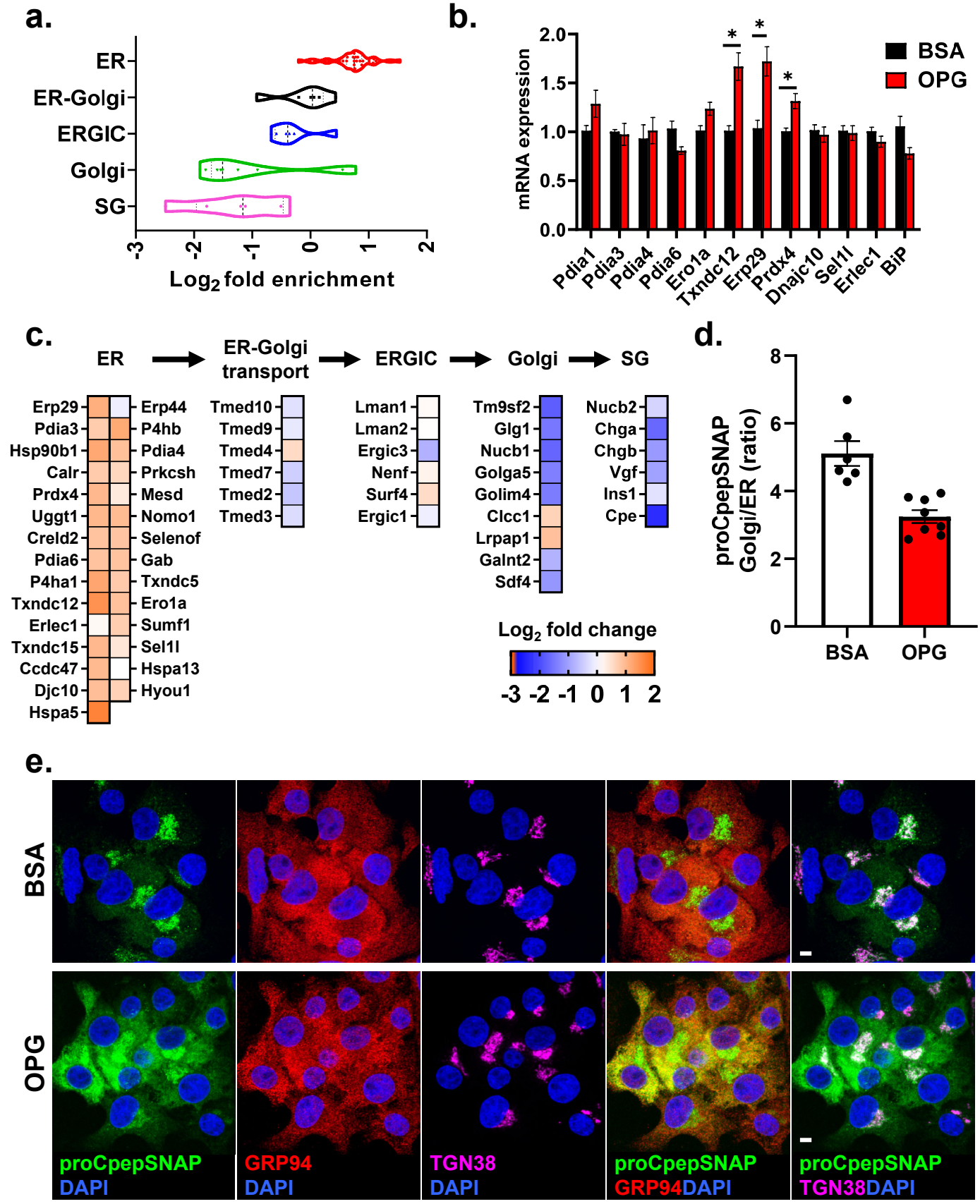
a.
ER
ER-Golgi
ERGIC
Golgi
SG
-3
-2
-1
0
1
2
Log2 fold enrichment
b.
mRNA expression
2.0
1.5
1.0
0.5
0.0
BSA
OPG
Pdia1
Pdia3
Pdia4
Pdia6
Ero1a
Txndc12
Erp29
Prdx4
Dnajc10
Sel1l
Erlec1
BiP
c.
ER
ER-Golgi transport
ERGIC
Golgi
SG
Erp29
Pdia3
Hsp90b1
Calr
Prdx4
Uggt1
Creld2
Pdia6
P4ha1
Txndc12
Erlec1
Txndc15
Ccdc47
Djc10
Hspa5
Erp44
P4hb
Pdia4
Prkcsh
Mesd
Nomo1
Selenof
Gab
Txndc5
Ero1a
Sumf1
Sel1l
Hspa13
Hyou1
Tmed10
Tmed9
Tmed4
Tmed7
Tmed2
Tmed3
Lman1
Lman2
Ergic3
Nenf
Surf4
Ergic1
Tm9sf2
Glg1
Nucb1
Golga5
Golim4
Clcc1
Lrpap1
Galnt2
Sdf4
Nucb2
Chga
Chgb
Vgf
Ins1
Cpe
Log2 fold change
-3 -2 -1 0 1 2
d.
proCpepSNAP Golgi/ER (ratio)
8
6
4
2
0
BSA
OPG
e.
BSA
OPG
proCpepSNAP
DAPI
GRP94
DAPI
TGN38
DAPI
proCpepSNAP
GRP94DAPI
proCpepSNAP
TGN38DAPI

Figure 5.

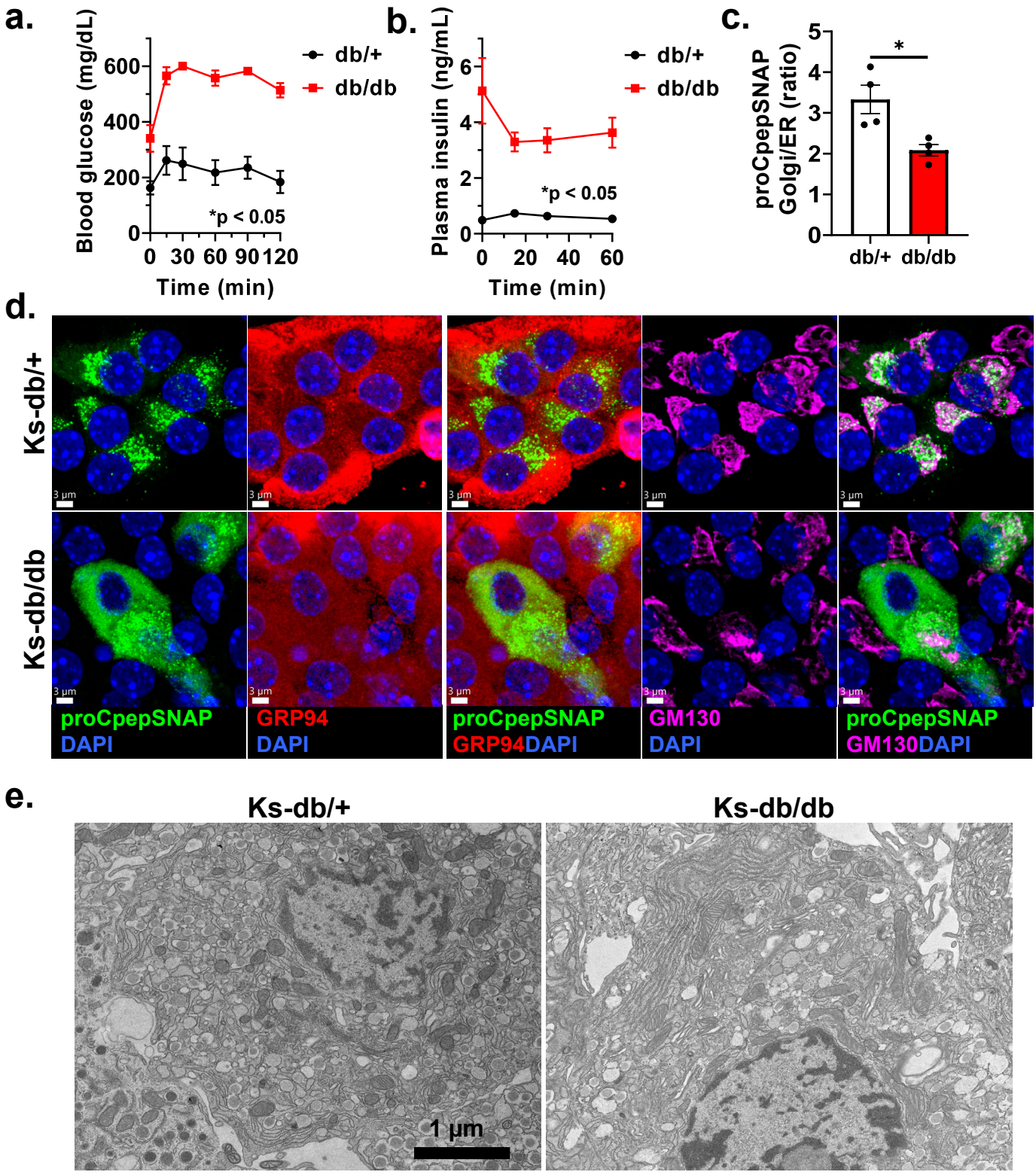
a.
Blood glucose (mg/dL)
600
400
200
0
0 30 60 90 120
Time (min)
db/+
db/db
*p < 0.05
b.
Plasma insulin (ng/mL)
6
4
2
0
0 20 40 60
Time (min)
db/+
db/db
*p < 0.05
c.
proCpepSNAP Golgi/ER (ratio)
5
4
3
2
1
0
*
db/+ db/db
d.
Ks-db/+
Ks-db/db
3 µm
proCpepSNAP
DAPI
GRP94
DAPI
proCpepSNAP
GRP94DAPI
GM130
DAPI
proCpepSNAP
GM130DAPI
e.
Ks-db/+
Ks-db/db
1 µm

Figure 6.

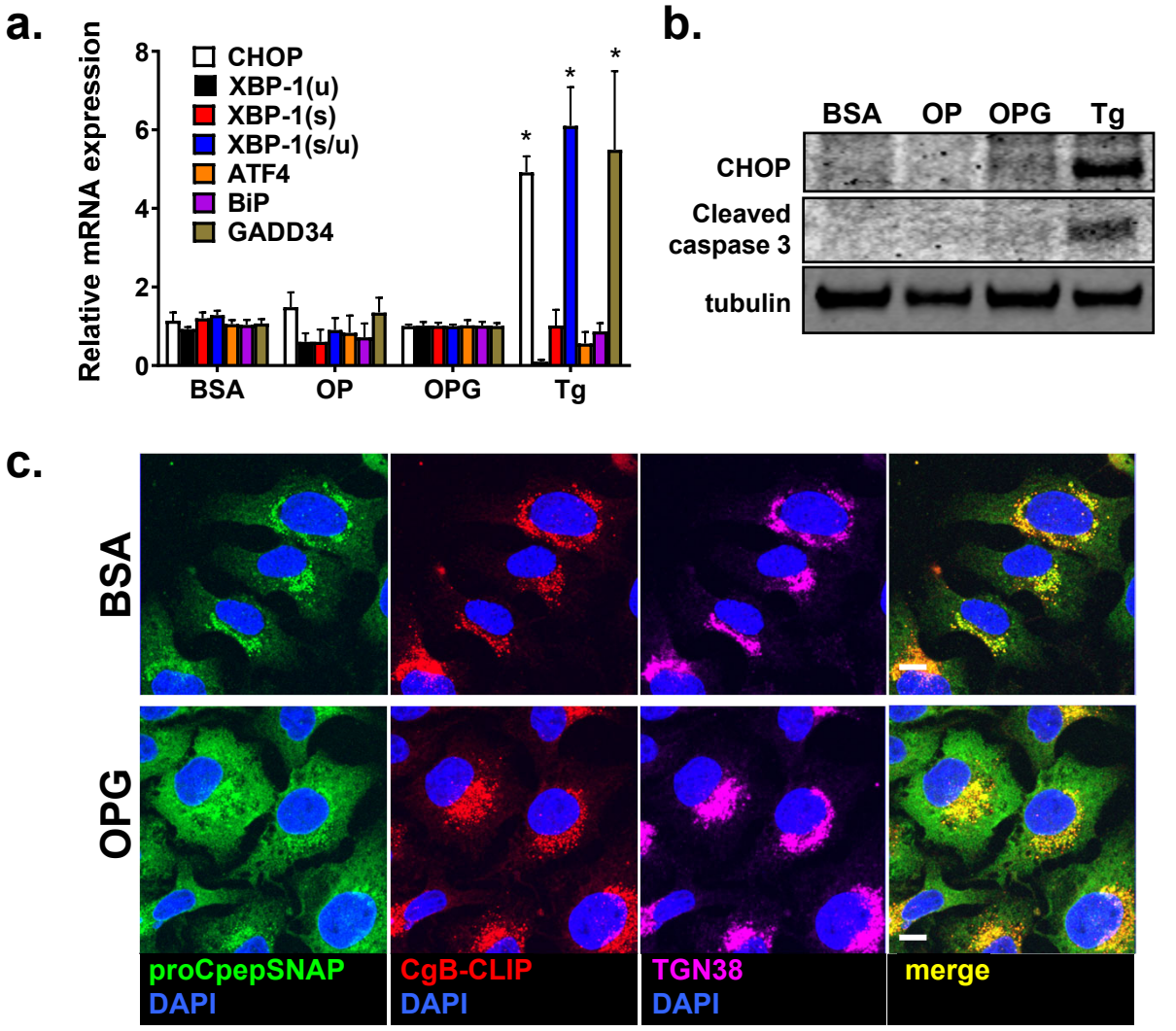
a.
Relative mRNA expression
CHOP
XBP-1(u)
XBP-1(s)
XBP-1(s/u)
ATF4
BiP
GADD34
BSA
OP
OPG
Tg
b.
BSA
OP
OPG
Tg
CHOP
Cleaved caspase 3
tubulin
c.
BSA
OPG
proCpepSNAP
DAPI
CgB-CLIP
DAPI
TGN38
DAPI
merge

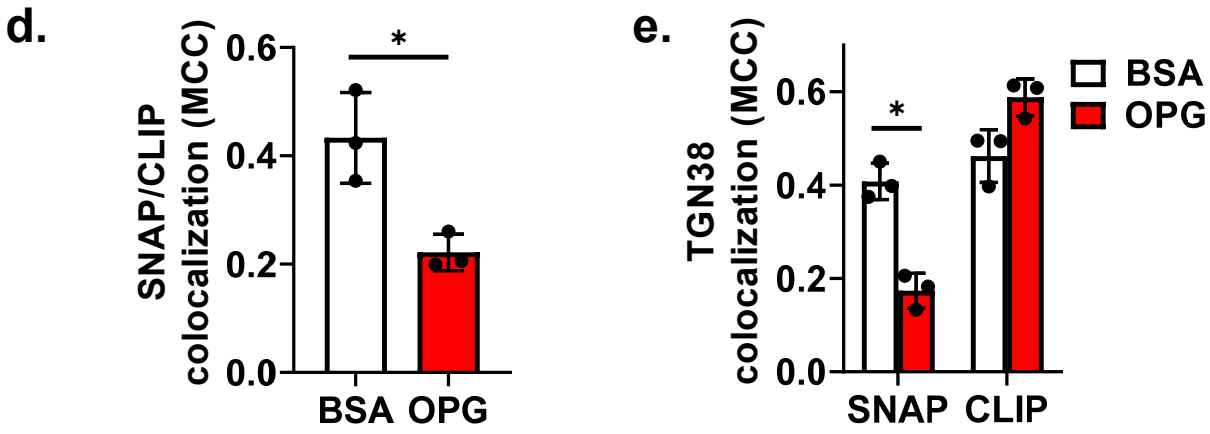
d.
SNAP/CLIP colocalization (MCC)
BSA
OPG
e.
TGN38 colocalization (MCC)
SNAP
CLIP
BSA
OPG

Figure 7.

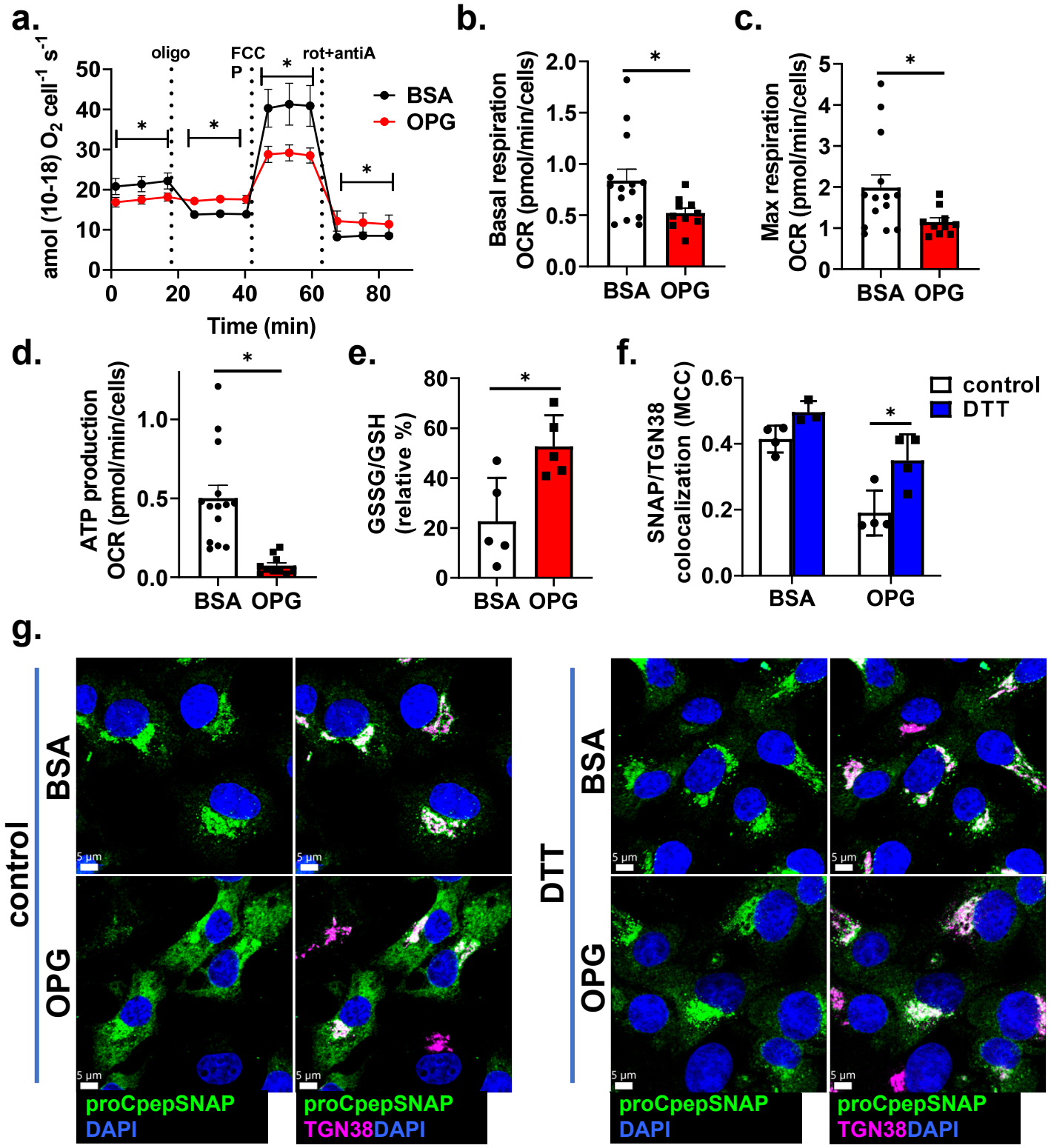
a.
amol (10-18) O2 cell-1 s-1
oligo
FCCP
rot+antiA
BSA
OPG
Time (min)
b.
Basal respiration OCR (pmol/min/cells)
BSA
OPG
c.
Max respiration OCR (pmol/min/cells)
BSA
OPG
d.
ATP production OCR (pmol/min/cells)
BSA
OPG
e.
GSSG/GSH (relative %)
BSA
OPG
f.
SNAP/TGN38 colocalization (MCC)
control
DTT
BSA
OPG
g.
control
DTT
BSA
OPG
5 µm
proCpepSNAP
DAPI
TGN38

Figure 8.

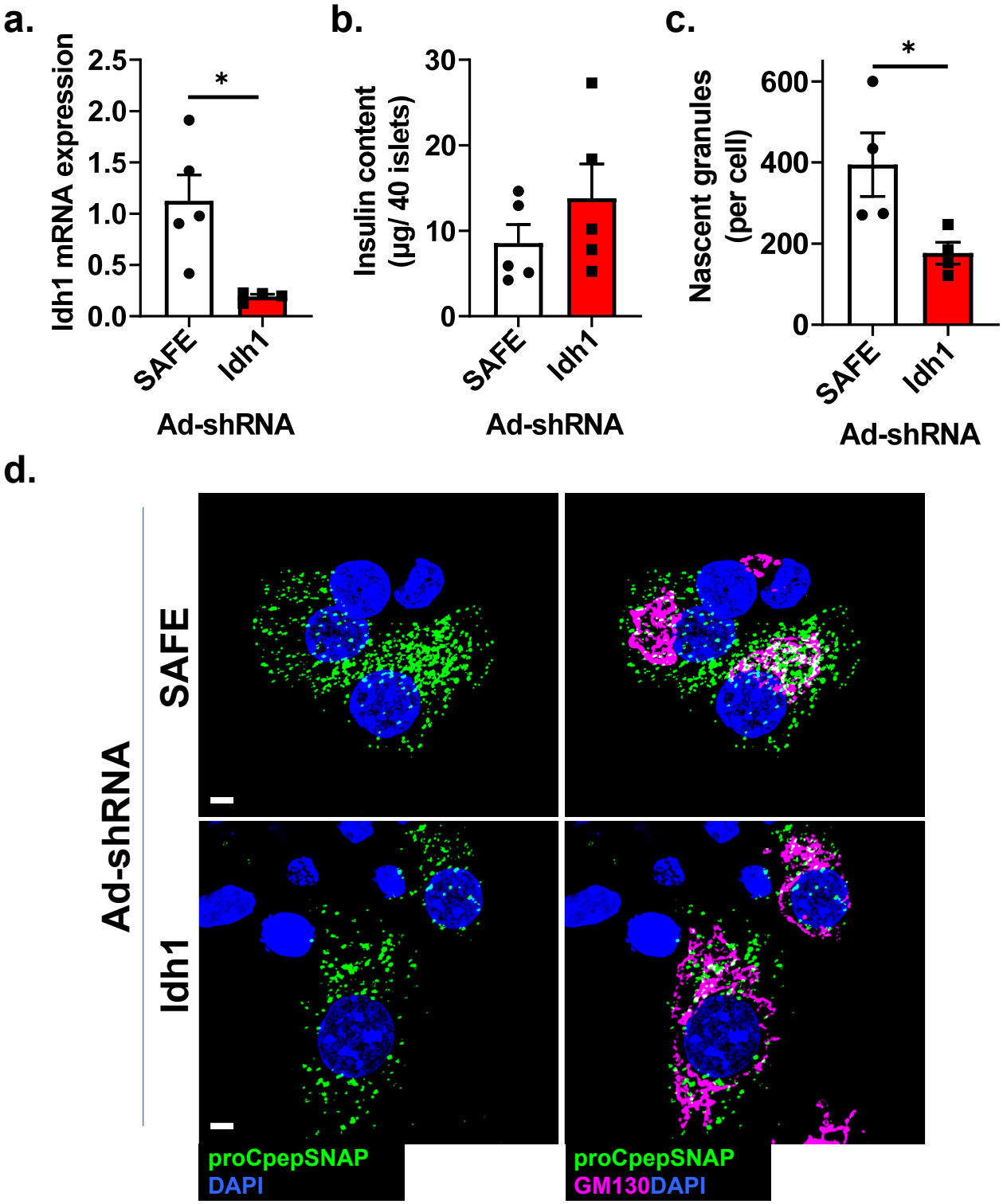
a.
Idh1 mRNA expression
2.5
2.0
1.5
1.0
0.5
0.0
*
SAFE
Idh1
Ad-shRNA
b.
Insulin content
(µg/ 40 islets)
30
20
10
0
SAFE
Idh1
Ad-shRNA
c.
Nascent granules
(per cell)
600
400
200
0
*
SAFE
Idh1
Ad-shRNA
d.
Ad-shRNA
SAFE
Idh1
proCpepSNAP
DAPI
proCpepSNAP
GM130DAPI

Figure 9.

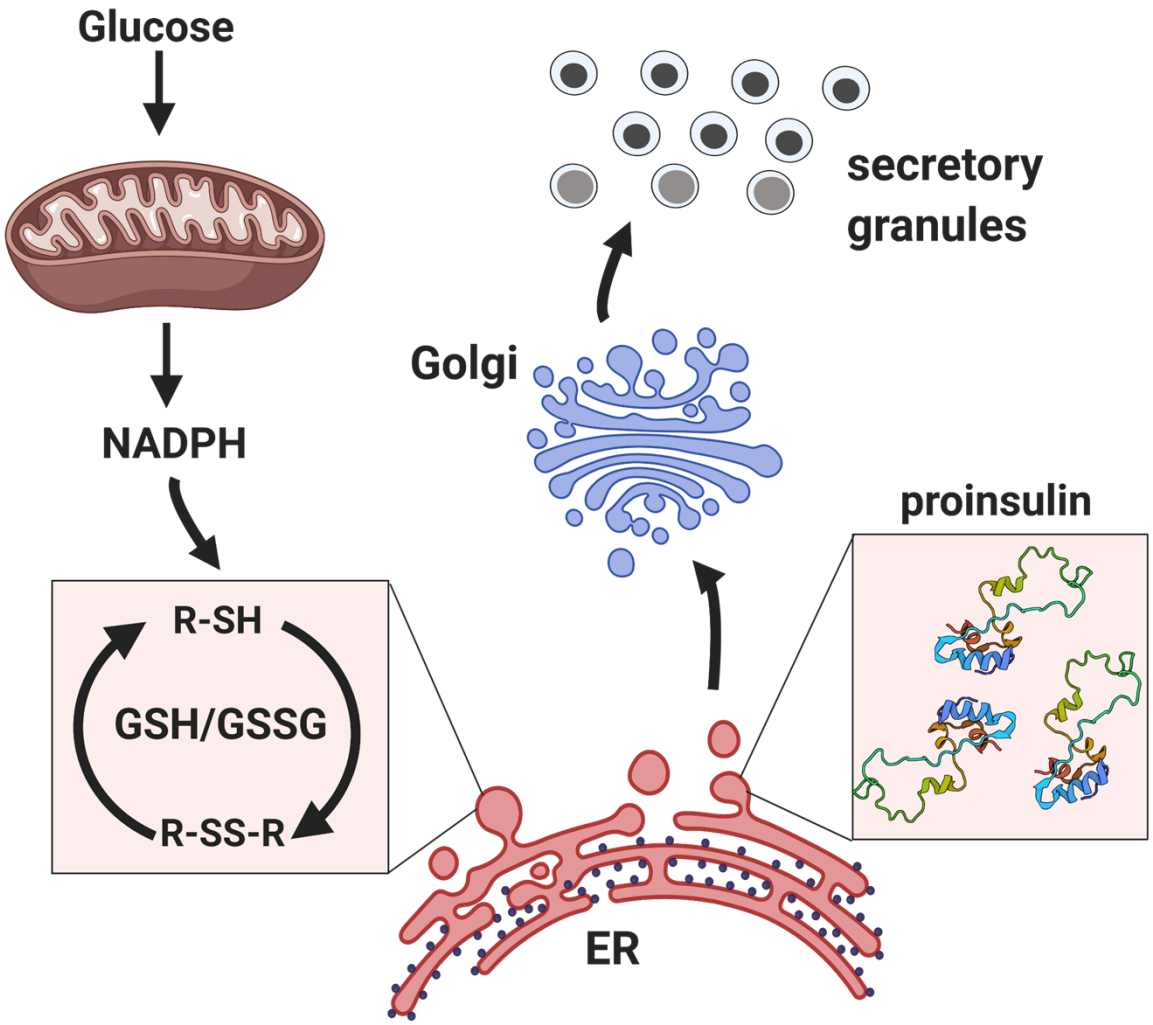
Glucose
NADPH
R-SH
GSH/GSSG
R-SS-R
Golgi
secretory
granules
proinsulin
ER